

## QZO: A Catalog of 5 Million Quasars from the Zwicky Transient Facility

S. J. NAKONECZNY,<sup>1</sup> M. J. GRAHAM,<sup>1</sup> D. STERN,<sup>1</sup> G. HELOU,<sup>1</sup> S. G. DJORGOVSKI,<sup>1</sup> E. C. BELLM,<sup>2</sup> T. X. CHEN,<sup>3</sup>  
R. DEKANY,<sup>4</sup> A. DRAKE,<sup>1</sup> A. A. MAHABAL,<sup>1,5</sup> T. A. PRINCE,<sup>1</sup> R. RIDDLE,<sup>4</sup> B. RUSHOLME,<sup>3</sup> AND N. SRAVAN<sup>6</sup>

<sup>1</sup>*Division of Physics, Mathematics and Astronomy, California Institute of Technology, Pasadena, CA 91125, USA*

<sup>2</sup>*DIRAC Institute, Department of Astronomy, University of Washington, Seattle, WA 98195, USA*

<sup>3</sup>*IPAC, California Institute of Technology, Pasadena, CA 91125, USA*

<sup>4</sup>*Caltech Optical Observatories, California Institute of Technology, Pasadena, CA 91125, USA*

<sup>5</sup>*Center for Data Driven Discovery, California Institute of Technology, Pasadena, CA 91125, USA*

<sup>6</sup>*Department of Physics, Drexel University, Philadelphia, PA 19104, USA*

### ABSTRACT

Machine learning methods are well established in the classification of quasars (QSOs). However, the advent of light curve observations adds a great amount of complexity to the problem. Our goal is to use the Zwicky Transient Facility (ZTF) to create a catalog of QSOs. We process the ZTF DR20 light curves with a transformer artificial neural network and combine the Pan-STARRS (PS), AllWISE, and Gaia surveys with extreme gradient boosting. Using ZTF  $g$ -band data with at least 100 observational epochs per light curve, we obtain 97% F1 score for QSOs. We find that with 3 day median cadence, a survey time span of at least 900 days is required to achieve 90% QSO F1 score. However, one can obtain the same score with a survey time span of 1800 days and the median cadence prolonged to 12 days. We find that ZTF classification is superior to the PS static bands, and on par with WISE and Gaia measurements. Additionally, we find that the light curves provide the most important features for QSO classification in the ZTF dataset. We robustly classify objects fainter than the  $5\sigma$  SNR limit at  $g = 20.8$  by requiring  $g < n_{\text{obs}}/80 + 20.375$ . For this sample, we run inference with added WISE observations, and find 4,849,574 objects classified as QSOs. For 33% of QZO objects, with available WISE data, we publish redshifts with estimated error  $\Delta z/(1+z) = 0.14$ . We release the catalog at: [placeholder<sup>a\)</sup>](#), and the code at: <https://github.com/snakoneczny/ztf-agn>.

*Keywords:* Active galactic nuclei — Astrominformatics — Catalogs — Classification — Large-scale structure of the Universe — Light curves — Light curve classification — Neural networks — Photometry — Time domain astronomy — Time series analysis — Quasars

### 1. INTRODUCTION

Quasars are a type of active galaxy, usually occupying massive dark matter halos (Eftekharzadeh et al. 2015; DiPompeo et al. 2016), and emitting enormous amounts of energy through accretion of matter onto a supermassive black hole (Kormendy & Ho 2013). They mostly appear as faint and point like objects. Due to their highly biased tracing of vast volumes of the large scale structure (DiPompeo et al. 2014; Laurent et al. 2017), quasars are used for various cosmological applications: a

test of the cosmological principle of isotropy and homogeneity (Secrest et al. 2021; Dam et al. 2023), the growth rate of structure (García-García et al. 2021; Alonso et al. 2023), primordial non-Gaussianity (Leistedt et al. 2014; Castorina et al. 2019; Krolewski et al. 2024), the Hubble distance (Hou et al. 2020), baryon acoustic oscillations (Ata et al. 2017; Zarrouk et al. 2021), the integrated Sachs-Wolfe effect (Stölzner et al. 2018), the expansion rate of the universe as standardizable candles (Setti & Woltjer 1973; Risaliti & Lusso 2015; Lusso et al. 2020), calibration of the reference frames for Galactic studies (Lindgren et al. 2018), measurement of halo masses (DiPompeo et al. 2017), cross-correlation with the  $\gamma$ -ray background (Cuoco et al. 2017), tomographic angular clustering (Leistedt et al. 2014; Ho et al. 2015),

Corresponding author: Szymon J. Nakoneczny  
[nakonecz@caltech.edu](mailto:nakonecz@caltech.edu)

<sup>a)</sup> Data will be published upon acceptance in a journal.

quasar bias measurements (Sherwin et al. 2012), the baryon density (Yahata et al. 2005), cosmic magnification (Scranton et al. 2005), and cross correlation with foreground galaxies as a probe of weak lensing (Ménard & Bartelmann 2002).

Quasars are also variable objects well described by a damped random walk (Kelly et al. 2009; Kozłowski et al. 2010; MacLeod et al. 2010). However, there are also fluctuations in a form of, e.g. tidal disruption events (TDEs, Rees 1988; Gezari 2021; Stein et al. 2024), and possibly gravitational wave (GW) flares (McKernan et al. 2019; Graham et al. 2020; Wang et al. 2021; Kimura et al. 2021; Perna et al. 2021). The latter have not yet been confirmed, but Graham et al. (2023) present nine candidate counterparts for such events from Ligo/Virgo detectors (LIGO Scientific Collaboration et al. 2015; Acernese et al. 2015). The importance of such events results from accretion disks being the only channel for stellar mass black hole mergers which reliably produce electromagnetic (EM) counterparts, and thus the identification of GW event with a host galaxy at a known redshift (Ash-ton et al. 2021; Calderón Bustillo et al. 2021; Palmese et al. 2021). The GW signal then becomes a standard siren, which can be used to measure the expansion history of the universe (Mukherjee et al. 2020; Chen et al. 2022). However, detection of EM counterparts in AGN (active galactic nucleus) time series is challenging due to potentially too bright or too thick accretion disks, as well as the incomplete census of AGN. Hence, a first step in a systematic search of such flares is a construction of AGN catalog with available time-series data.

The most reliable source of quasar<sup>1</sup> identification and redshifts are galaxy spectra. Spectroscopic surveys have provided  $\sim 10^5$ - $10^6$  QSOs, e.g. 2dF QSO Redshift Survey (2QZ, Croom et al. 2004), 2dF-SDSS LRG and QSO (2SLAQ, Croom et al. 2009), and the Sloan Digital Sky Survey (SDSS, York et al. 2000; Lyke et al. 2020). Ongoing and future spectroscopic surveys such as DESI (DESI Collaboration et al. 2016) and 4MOST (de Jong et al. 2019; Merloni et al. 2019; Richard et al. 2019) expect to obtain spectra for 3 million quasars. Since QSOs are sparsely distributed in comparison to inactive galaxies, wide area photometric surveys are a much better way of observing large numbers of QSOs. However, the lack of spectra makes classification more complicated and redshifts much less accurate. Nearly 3 million quasars with photometric redshifts (photo-zs) have been cataloged (e.g. Shu et al. 2019; Kunsági-Máté et al. 2022; Storey-Fisher et al. 2024), through

surveys such as the Wide-field Infrared Survey Explorer (WISE, Wright et al. 2010), unWISE (Lang 2014), Pan-STARRS (Chambers et al. 2016), and Gaia (Gaia Collaboration et al. 2016). In the future, the Rubin Observatory’s LSST will photometrically observe up to 10 million quasars (Ivezić 2016).

One possibility to classify objects in photometric data is SED fitting, which depending on available data can derive physical properties (Ciesla et al. 2015; Stalevski et al. 2016; Calistro Rivera et al. 2016; Yang et al. 2020; Malek et al. 2020), as well as photo-zs (Salvato et al. 2009, 2011; Fotopoulou et al. 2016; Fotopoulou & Paltani 2018). Also, using different magnitudes, one can create a color-color space which allows for object classification (Warren et al. 2000; Maddox et al. 2008; Edelson & Malkan 2012; Stern et al. 2012; Wu et al. 2012; Secrest et al. 2015; Assef et al. 2018). More sophisticated methods include probabilistic models (Richards et al. 2004, 2009a,b; Bovy et al. 2011, 2012; DiPompeo et al. 2015; Richards et al. 2015), but due to the high complexity of multidimensional color-color space, machine learning (ML) methods achieve the best results (Brescia et al. 2015; Carrasco et al. 2015; Kurcz et al. 2016; Nakoneczny et al. 2019; Logan & Fotopoulou 2020). Depending on the availability of infrared observations, one can also estimate photo-zs with ML (Brescia et al. 2013; Yang et al. 2017; Pasquet-Itam & Pasquet 2018; Curran 2020; Nakoneczny et al. 2021).

Another type of photometric observation are time series data, provided by surveys such as ASAS (Pojmanski 2002), NSVS (Woźniak et al. 2004; Hoffman et al. 2009), the Palomar Transient Factory (Law et al. 2009), the Catalina Surveys (Drake et al. 2014, 2017), and ASAS-SN (Kochanek et al. 2017; Jayasinghe et al. 2018). The Zwicky Transient Facility (ZTF, Bellm et al. 2019a; Graham et al. 2019; Masci et al. 2019; Dekany et al. 2020) has operated since March 2018 and covers the northern sky with 3 day cadence. Within the time-series data, ML was applied to classify microlensing events (Godines et al. 2019), transients (Stachie et al. 2020; Gomez et al. 2023; Rehemtulla & Miller 2023), and variables (Richards et al. 2011; García-Jara et al. 2022; Mistry et al. 2022). The ZTF Source Classification Project (SCoPe, van Roestel et al. 2021; Coughlin et al. 2021; Healy et al. 2024) provides classification for many different classes of variables. However, our goal is to create a method fully optimized for quasar detection, apply deep learning methods, and achieve the highest possible accuracy. Observations of quasar light curves are relatively new, and their usage in classification has not yet been fully established in comparison to other astronomical observations. ZTF is well suited for this goal, as it

<sup>1</sup> We use AGN and QSO terms interchangeably.

delivers light curves with irregular sampling, over a six year period of observations.

Our first goal is to test quasar classification with deep learning methods based on the transformer architecture, and compare the results with shallow feature extraction methods. Next, we establish the minimum requirements on the length and sampling of time-series data in order to achieve reliable quasar classification. We compare ZTF classification to visible *griz* bands from Pan-STARRS DR1 (PS, Chambers et al. 2016), mid-infrared W[1-4] filters from AllWISE (Wright et al. 2010; Mainzer et al. 2011; Cutri et al. 2021), and parallax and proper motion measurements from Gaia EDR3 (Gaia Collaboration et al. 2016, 2021). Finally, we use these results to create a high quality quasar catalog based on the ZTF data.

The paper is structured as follow. Section 2 presents the ZTF survey, as well as inference and training data for the ML models. Section 3 presents the ML models, evaluation methods, and experimental methodology. Section 4 presents the results, while Section 5 briefly discusses spectroscopy obtained at Palomar Observatory of sources with conflicting SDSS and machine learning classifications. Finally, Section 6 interprets and concludes the work. Unless stated otherwise, we present the results for the ZTF *g*-band data.

## 2. DATA

### 2.1. Zwicky Transient Facility

ZTF is an optical time domain survey operated at the Palomar 48 inch Schmidt telescope since March 2018. Typical limiting magnitudes in *g* and *r* bands are 20.8 and 20.6, respectively. During its initial phase, its public surveys observed 27,500 square degrees over the northern sky, with a three night cadence, and 1000 to 2000 square degrees at the Galactic plane, with a one night cadence (Bellm et al. 2019b). Since December 2020, the ZTF second phase, the northern sky has been observed every two nights. Additional private surveys have sampled the sky with more specialized cadences, such as continuous single-field “deep drilling” observations. The data processing and access is available through the Science Data System at the Infrared Processing and Analysis Center (IPAC, Masci et al. 2019). The primary science goals of ZTF are the physics of supernovae and relativistic explosions, multi-messenger astrophysics, supernova cosmology, active galactic nuclei, TDEs, stellar variability, and solar system objects (Graham et al. 2019).

### 2.2. Inference data

We perform the inference using ZTF data release (DR) 20, covering March 2018 to January 2024. For inference, we use only the *g*-band data, while we add the *r*-band to experiments, and omit the *i*-band due to its much lower coverage compared to the two other bands. In total, ZTF DR20 consists of 1.5B and 2.4B objects in the *g*- and *r*-bands, respectively. The estimated number of bad epochs per light curve, with likely suspect and unusable photometry, is 8% and 11% in *g* and *r*, respectively<sup>2</sup>. We remove deep drilling observations by averaging observations within the same night. Finally, after removal of light curves with less than 20 observations, we obtain the inference dataset of 789M objects in the ZTF *g* band. Additionally, we either mark or remove duplicated light curves by finding objects which within 1'' have a neighbor with more observation epochs. The number of deduplicated light curves equals 533M.

### 2.3. Training data

We obtain the training data in *g* and *r* bands by cross-matching the ZTF data with SDSS DR18 (SDSS, Almeida et al. 2023), using a 1'' distance threshold, and applying the same preprocessing as in the case of inference data. We clean the SDSS data by removing objects with known redshift estimation errors as encoded in the *zWarning* flag, with the exception of the fifth bit of this flag, which does not signal problems. Additionally, we remove duplicated ZTF light curves by accepting only the longest light curve among the neighbors within the 1'' distance. We analyze both *g*- and *r*-band datasets independently. The training set size is 483k and 665k in *g*- and *r*-bands. The class distribution is 47% galaxies, 25% quasars, and 28% stars in the *g*-band, and 59% galaxies, 19% quasars, and 22% stars in the *r*-band. It totals to 645062 and 703685 quasars in *g*- and *r*-bands, respectively. We compute the experiments with shallow precomputed features (Healy et al. 2024) in Section 4.1, based on ZTF DR5, published in January 2021, since at the time of writing, shallow features were only computed for this DR. However, we did not first utilize all the light curves from this dataset, and could not update it later due to removal of data from the servers. Hence, the DR5 training dataset size is 301k and 381k in *g*- and *r*-bands, respectively, which also lowers the deep learning results due to a smaller training set size. We use the DR5 data only for comparison between the shallow and deep learning results of light curve classification. We use 37 of the precomputed features, omitting the

<sup>2</sup> See Table 1 in [https://irsa.ipac.caltech.edu/data/ZTF/docs/releases/dr20/ztf\\_release\\_notes\\_dr20.pdf](https://irsa.ipac.caltech.edu/data/ZTF/docs/releases/dr20/ztf_release_notes_dr20.pdf)

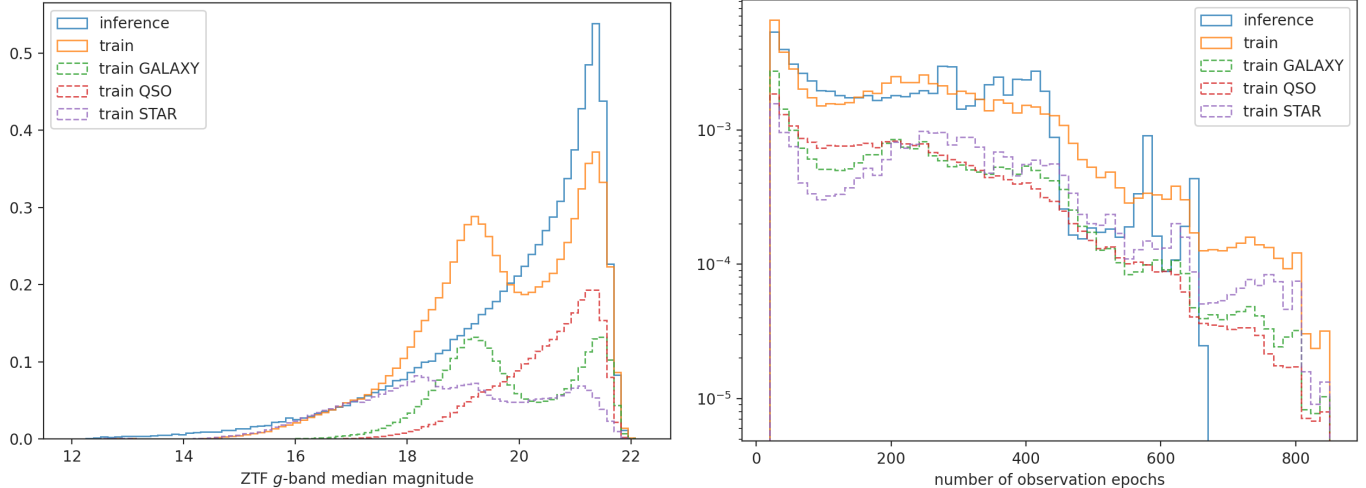


**Figure 1.** Distributions of median  $g$ -band magnitude and number of observation epochs for the inference (blue), training (orange), and each class component of the training data (green, red, and purple). The inference and training distributions are normalized to unity, and the class distributions are normalized to one third.

magnitude-time histograms and ZTF alerts information (see Table 1 in Healy et al. 2024).

Figure 1 shows distributions of median magnitude and number of observations for inference and training data, also separated for different classes. The plots are normalized to unity, and the class plots are divided by three in order to properly compare between the different classes. We see on the magnitude plot that the training data cover the inference data, but the training distribution is different from the inference one, which together with the class distribution, hint to a larger fraction of quasars present at the faint end of inference data. Due to this, the final classification of inference data requires additional testing, and the results will not be calibrated, meaning that among objects with estimated QSO probability around 90%, the actual number of quasars will be different than the 90%. The number of observations plot shows that there are no significant differences between the classes. Such differences could constitute a data leak, as it could be used as additional information for classification, which in fact might not be the same in the inference data.

#### 2.4. Other surveys

We compare the ZTF based classification with AllWISE, Gaia EDR3, and PS DR1 by cross-matching the ZTF training datasets in  $g$ - and  $r$ -bands using a  $1''$  matching distance. From PS, AllWISE, and Gaia, we use  $griz$ ,  $W[1-4]$ , and  $g$ ,  $bp$ ,  $rp$  magnitudes, respectively. We add colors from all magnitude pair combinations within each survey. Additionally, we add parallax and proper motion measurements from Gaia. We do not use

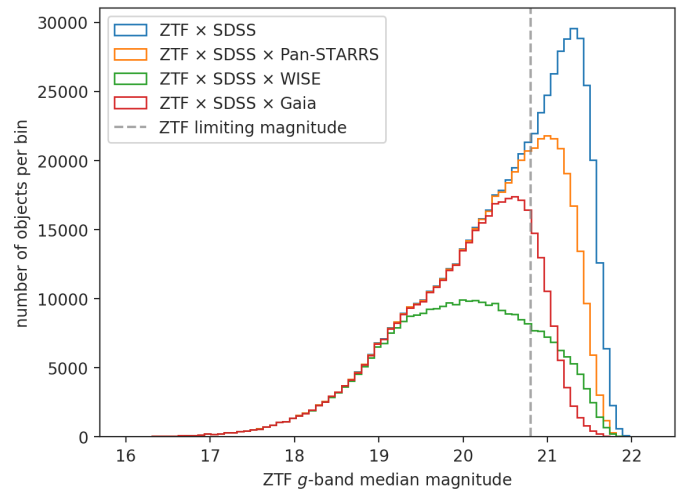


**Figure 2.** Number of quasars available in the training sample (blue), and its cross-matches with PS (orange), WISE (green) and Gaia (red). The vertical line shows the ZTF’s magnitude limit, while for the other surveys, we apply limiting magnitude cuts as described in Section 2.4. We note that the final catalog has no magnitude cuts on WISE survey.

error measurements for any of the features, either as inputs or weights for loss functions. Requiring availability of all the cross-matched features, we obtain the following subsets of the ZTF  $g$ -band training data: ZTF x PS 98%, ZTF x WISE 77%, ZTF x Gaia 45%. When comparing the classification based on different surveys, we apply the magnitude limits: PS  $griz$  22.0, 21.8, 21.5,



20.9, WISE W[1-2] 17.1, 15.7, Gaia  $g$  21, respectively. Fig. 2 shows a comparison of quasar distributions between the full training sample and the cross-matched subsets. We also cross-match with AllWISE for the inference data, as justified in Sections 4.2 and 4.3. For simplicity, we use WISE to refer to the AllWISE sample.

### 3. METHODOLOGY

#### 3.1. *Astromer*

We classify the light curves using Astromer (Donoso-Oliva et al. 2023), a deep learning transformer architecture, pre-trained on all the ZTF DR10  $g$ -band data. The model uses attention layers trained in a semi supervised way by removing random windows from the light curves, and then recreating the missing parts. The model is limited to 200 input observation epochs, transforming each observation into a vector of 256 tokens, which results in an encoder output size of  $200 \times 256$ . We fine-tune the model for a classification task by processing the encoder output with other types of layers.

#### 3.2. *Pipeline*

We test the ML models with a random 80%, 10%, 10% split for the training, validation and test sample, respectively. We always use the same split for fine tuning Astromer, training the classification network, and making ensembles with other surveys. We use two metrics to evaluate the classification: the general three class accuracy defined as a fraction of correctly classified objects, and QSO F1 score defined as a harmonic mean of QSO completeness and precision.

We first retrain Astromer using its original training procedure on the  $g$ - and  $r$ -band training data, which do not contain the deep drilling observations unlike the original Astromer training. For the  $r$ -band, this step involves transfer learning from the  $g$ -band. Hence, the retraining for  $r$ -band is about 3 times longer. We find that retraining the transformer model provides better results for the final classification task, and allows for faster training and experimentation with the classification models. We then tested the retrained Astromer for classification with different combinations of convolutional, long short-term memory (LSTM, Hochreiter & Schmidhuber 1997), normalization, and dense layers, ranging from 2048 to 128 neurons, as well as reduction of the transomer embeddings to mean, maximum or minimum values. We find that the best results are achieved with the following architecture: mean reduction of the embeddings, 1024, 512 and 256 neuron dense layers with the rectified linear unit activation function (ReLU, Agarap 2018), normalization layer, and three

neuron output layer. For training, we use the Adam optimizer with a 0.001 learning rate, scheduled to 0.0005 at epoch 4, and 0.0001 at epoch 9. After training the artificial neural network (ANN) classification models on  $g$ - and  $r$ -bands, we use extreme gradient boosting (XGB, Chen & Guestrin 2016) to ensemble the deep learning classifications with features from the PS, WISE and Gaia surveys. We use the same XGB training parameters as found optimal in a similar classification task in Nakoneczny et al. (2021). We also test adding the features from other surveys as additional inputs to fully connected layers of the ANN, but find this approach to provide worse results. Also, ensembling with XGB allows separation of the ANN training from the final classification models, enabling for easier and faster comparisons with other surveys.

### 4. RESULTS

#### 4.1. *Light curve classification*

Since ZTF data span a wide range of magnitudes and observation epochs, we start by analyzing how the classification scores depend on those factors. Fig. 3 shows the dependence of ZTF  $g$ -band QSO F1 score on the number of observation epochs and magnitude. We find that given at least 50 observation epochs, the QSO F1 scores deteriorates by 10pp between the objects at magnitude limit  $g \sim 20.8$  and the faintest data points at  $g \sim 21.5$ . We can remove the objects with lower classification quality by applying the dashed red line cut at  $g < n_{\text{obs}}/80 + 20.375$ . Table 1 shows the scores for different combinations of limiting magnitude and minimum number of observation epochs. The cuts enable better F1 scores within the catalog, but taking into account the total loss of objects due to cuts, we observe a deterioration in the global QSO F1 scores. The suggested red line cut allows to achieve 93% QSO F1 score, with the global metric equal 85%. Fig. 4 shows detailed relations between QSO F1 score, magnitude, number of observation epochs and redshift for the ZTF  $\times$  PS training data. We observe that the PS data improves the classification results at the faint end, mostly due to the deeper photometry provided by PS. At brighter magnitudes we observe superiority in ZTF classification over PS. We see that the Astromer’s limit of 200 observation epochs does not allow us to probe further increases in scores for more observing epochs. These tests analyze the ZTF classification outputs, but with their weakness that low numbers of objects at certain values, as shown by the gray dashed lines in the Fig. 4, can result in

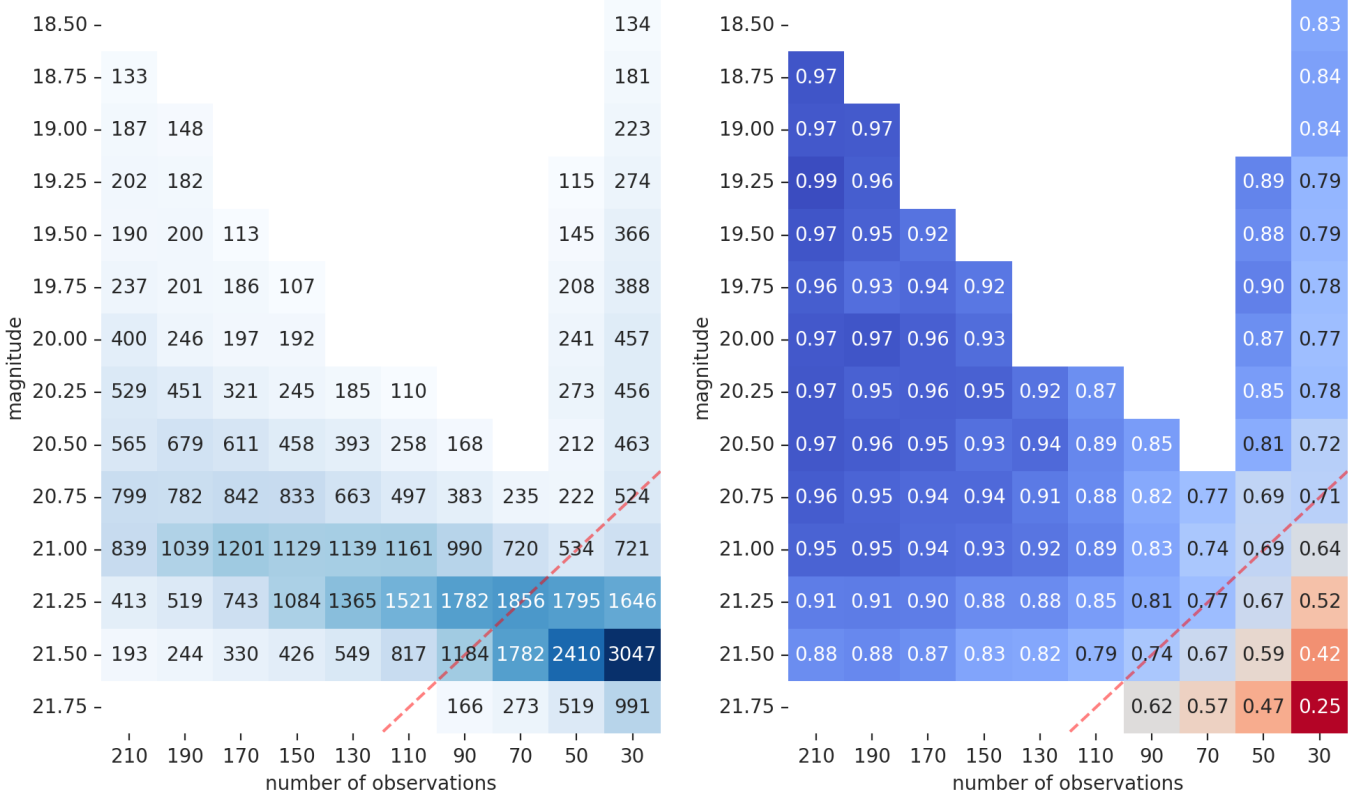


**Figure 3.** Number of QSOs (*left*) and QSO F1 scores (*right*) for the ZTF  $g$ -band XGB model based on transformer classifications and median magnitudes as features. We show the results in equally sized and non overlapping bins of the number of observations ( $x$  axis) and  $g$ -band magnitude ( $y$  axis), where the ticks mark centers of the bins.

under-performing models due to a lack of training data with specific characteristics.

In order to perform unbiased analysis of relations between classification scores, time span and number of observation epochs, we create training datasets of constant time span and number of observation epochs within all light curves, and train transformer models on each such training set. We create these datasets by taking light curves with time span higher than 1800 days and number of observations higher than the median value. Then, we limit the number of observations to 100%, 80%, 60%, 40%, 20%, 10% and 5% of the median value, which defines the median cadence. Finally, we limit the timespan by removing specific windows of observation epochs from heads of light curves. Fig. 5 shows the results of those tests. We observe strong dependence, and results higher than 90% obtained either at 900 day time span at the highest 3 day cadence, or the longest 1800 day time span at a lowered 12 day cadence. However, even a 500 day time span or 30 day median cadence can provide results better than 80%.

We compare the deep learning transformer classification to the shallow ensemble classifier with precomputed features based on ZTF DR5. We observe a difference between 81% and 89% QSO F1 scores for the shallow and deep learning models, respectively. However, for a similar setup in ZTF DR20, transformer scores 95%, as shown in Table 1 (row 5), for a magnitude-limited sample. This difference is due to the dataset size and time span difference between DR5 and DR20. The dataset size difference would affect the shallow models less significantly than the deep learning models, hence, we might expect the total difference between shallow and deep learning models to be even larger than the one estimated from DR5.

#### 4.2. Comparison with other surveys

We use PS, WISE and Gaia to compare the light curve classification with other types of surveys. Table 2 presents a detailed comparison between the ZTF, PS, WISE and Gaia surveys. The results are calculated on the test data with applied limiting magnitudes and re-

**Table 1.** Classification results of the ZTF  $g$ -band XGB model based on transformer classifications and median magnitudes as features, for combinations of limiting magnitude defined by mean SNR higher than  $5\sigma$ , ZTF observation epochs greater than 100, and a custom cut as a function of both magnitude and number of observation epochs.

data cuts	$g$ -band				$r$ -band			
	QSO	QSO F1	accuracy	QSO	QSO F1	accuracy		
	fraction	full sample	subset	subset	fraction	full sample	subset	subset
(1)	(2)	(3)	(4)	(5)	(6)	(7)	(8)	(9)
none	1.00	<b>0.88</b>	0.88	0.88	1.00	<b>0.85</b>	0.85	0.89
$g < n_{\text{obs}}/80 + 20.375$	0.84	0.85	0.93	0.91	0.90	0.84	0.89	0.90
$\text{SNR} > 5\sigma \vee n_{\text{obs}} > 100$	0.79	0.83	0.94	0.92	0.84	0.82	0.90	0.91
$n_{\text{obs}} > 100$	0.73	0.80	0.95	0.93	0.76	0.79	0.92	0.92
$\text{SNR} > 5\sigma$	0.57	0.68	0.95	0.94	0.58	0.67	0.92	0.93
$\text{SNR} > 5\sigma \wedge n_{\text{obs}} > 100$	0.50	0.64	<b>0.97</b>	<b>0.95</b>	0.50	0.63	<b>0.95</b>	<b>0.94</b>

NOTE—‘QSO fraction’ gives a fraction of quasars after the cuts with respect to the full training sample in the first row, ‘QSO F1 full sample’ assumes negative classification for quasars excluded by the cuts, ‘QSO F1 subset’ takes into the account only objects left after the data cut, ‘accuracy subset’ stands for the general three class accuracy of subsets. Boldface shows the highest value in each column.

**Table 2.** XGB classification results on the ZTF  $g$ -band data cross-matched with other surveys. We apply limiting magnitude cuts for each survey, and require minimum number of ZTF observation epochs greater than 100. ZTF features include the transformer classifications and  $g$ -band median magnitude, while Section 4.2 describes features from the other surveys.

data	features	QSO	QSO F1	accuracy
		fraction	subset	subset
(1)	(2)	(3)	(4)	(5)
ZTF	ZTF	0.5	0.97	0.96
× PS	ZTF	0.49	0.97	0.96
	PS		0.82	0.90
	ZTF ⊕ PS		0.98	<b>0.99</b>
× Gaia	ZTF	0.48	0.97	0.97
	Gaia		0.96	0.97
	ZTF ⊕ Gaia		<b>0.99</b>	<b>0.99</b>
× WISE	ZTF	0.36	0.97	0.97
	WISE		0.98	0.93
	ZTF ⊕ WISE		<b>0.99</b>	<b>0.99</b>

NOTE—‘QSO fraction’ provides the fraction of QSOs present in the cross-matches with respect to the full ZTF training sample, and ‘accuracy’ stands for the general three class accuracy. Boldface shows the highest value in each column.

quire at least 100 ZTF observation epochs in order to minimize the magnitude differences between the surveys and compare their full predictive power. The comparison between ZTF and PS surveys shows 97% and 82% QSO F1 score, in favor of the light curve based classification. The results between ZTF, Gaia and WISE are similar, however, each of those surveys gains significant improvement when merging with the ZTF observations.

Table 3 shows the classification results of the full ZTF training sample, with features from other surveys added where available, and XGB processing the missing features where present. Adding PS, WISE, and Gaia features to the ZTF classification improves the QSO F1 scores by 7, 6, and 3 percent points, respectively. As shown in Section 4.1, in case of PS, the improvement is mostly at the faint end due to the PS fainter limiting magnitude.

Fig. 7 presents feature rankings from XGB models trained on all available features in two cases: all the ZTF data with processing of missing features, and a subset of objects detected by all surveys, with no missing features present. The rankings are based on binary QSO vs non-QSO classification to focus on the features important for QSO detection. The full ZTF sample measures the importance with regard to all available QSOs, but may potentially underestimate WISE importance, which is available for 72% of QSOs. On the other hand, the cross-match between all the surveys measures the

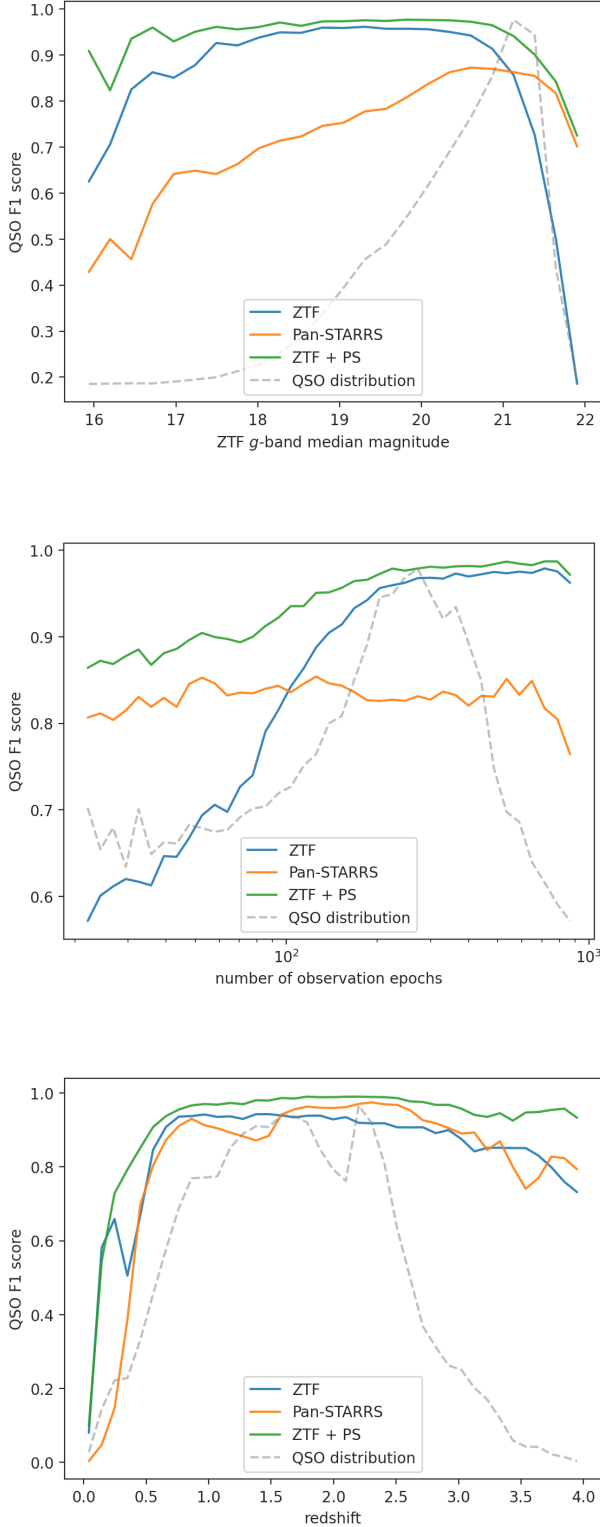


**Figure 4.** QSO F1 scores for the XGB  $g$ -band models trained on the ZTF  $\times$  PS data, as functions of median magnitude (top), number of ZTF observation epochs (middle), SDSS spectroscopic redshift (bottom). The gray dashed lines show overlaid quasar distributions. The models are trained using combinations of ZTF transformer classification, ZTF magnitude, and PS  $griz$  magnitudes and colors.

**Table 3.** XGB classification results on the ZTF  $g$ -band training data, with number of observation epochs greater than 20. In contrast to Table 2, here the XGB models classify objects with missing features from the other surveys.

features	QSO F1	accuracy
(1)	(2)	(3)
ZTF	0.88	0.88
ZTF $\oplus$ PS	0.95	0.96
ZTF $\oplus$ WISE	0.94	0.94
ZTF $\oplus$ Gaia	0.91	0.95
ZTF $\oplus$ PS $\oplus$ WISE	0.96	0.97
ZTF $\oplus$ PS $\oplus$ Gaia	0.96	<b>0.98</b>
ZTF $\oplus$ PS $\oplus$ WISE $\oplus$ Gaia	<b>0.97</b>	<b>0.98</b>

NOTE—‘Accuracy’ stand for the general three class accuracy. Boldface shows the highest value in each column.

feature importance only for red and point-like objects detectable by both the WISE and Gaia surveys. The top plot shows that the transformer’s QSO probability is the most important feature. The bottom plot shows that for the cross-matched data,  $W1 - W2$  color is the most important feature, but the transformer classification takes second place with 15% importance. Within the given set of surveys, parallax and proper motion measurements from Gaia are not the most important features.

#### 4.3. Redshift

We find that the light curves do not allow us to estimate redshifts for the quasars, and within the analyzed surveys, the WISE data are necessary to obtain the redshift estimates. Hence, for objects with available WISE data, we publish redshift estimates using XGB model trained on ZTF  $\times$  WISE data. Our measured error is  $\Delta z / (1 + z) = 0.14$ , with percentage of predictions more than 20% and 50% different then the spectroscopic redshift value equal 42% and 14%, respectively. The model uses ZTF  $g$ -band magnitude and WISE colors, but WISE colors are the most important features. Figure 8 shows the results of redshift estimation on the ZTF  $\times$  WISE test data.

#### 4.4. The catalog

According to the results from Sections 4.2 and 4.3, we publish the classification results based on the ZTF



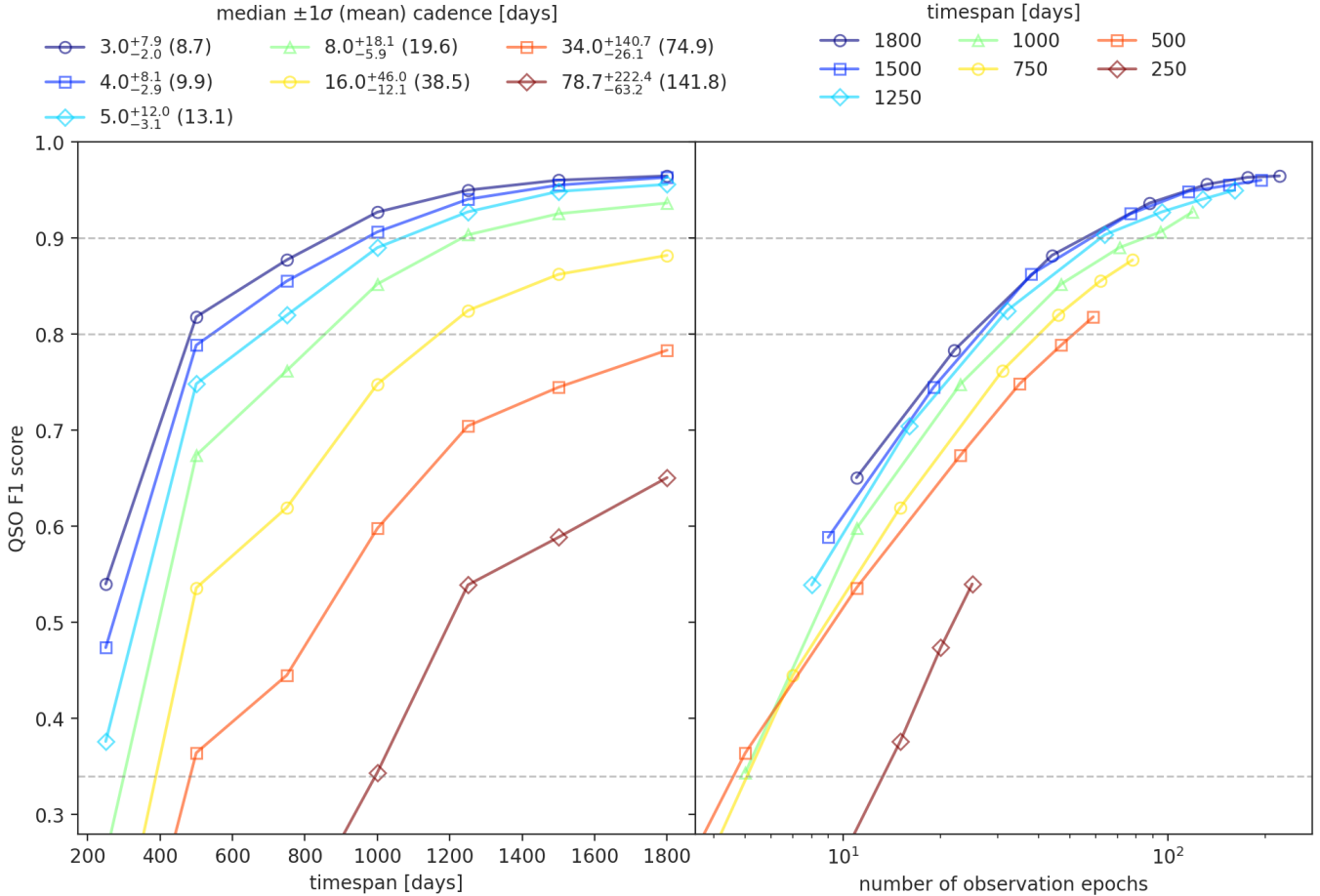


**Figure 5.** Transformer classification results on the ZTF  $g$ -band data as a function of limiting magnitude and with subsampled time span and number of observation epochs. Each score corresponds to a new training data and model, each training data has the same size, and each light curve within the given training data has the same time span and number of observations. To obtain lower cadences, we sample 100%, 80%, 60%, 40%, 20%, 10% and 5% of observation epochs, which corresponds to the successive lines on the left plot. Both plots show the same results: *left*: as a function of time span, and grouped for median cadence, *right*: as a function of number of observations, and grouped for time span.

and WISE surveys, together with the ZTF  $\times$  WISE redshift estimates. In the full ZTF catalog, we remove light curves which within  $1''$  have at least one neighbor with more observation epochs. This step removes duplicated light curves by choosing the ones with the highest number of observation epochs. Figure 9 and Table 4 show the resulting number of objects classified as QSOs at different data and classification probability cuts. The full catalog consists of 45.93 million objects classified as QSOs, but due to the class and magnitude distribution differences between the training and inference data, it is necessary to calibrate the resulting probabilities to achieve the same F1 score as estimated in the experiments, or establish a minimum classification probability to reduce QSO contamination by stars and galaxies, at a cost of lowered QSO completeness. From Section 4.1

we conclude that the highest quality QSO classification requires a cut based on magnitude and number of observation epochs at  $g < n_{\text{obs}}/80 + 20.375$ . At this cut, the estimated QSO F1 score equals 97%. Nakoneczny et al. (2019, 2021) uses a test based on Gaia parallaxes for a similar task of QSO classification based on SDSS data and suggests 90% minimum QSO classification probability. We obtain a limited catalog of higher purity by applying both the data and classification probability cuts, resulting in 4,849,574 objects classified as QSOs. We call this catalog QZO. However, the fainter sample below red line in fig 3 consists of many more true QSOs. Therefore, we also expect many more correctly classified QSOs below those limits, but with an unknown and higher contamination rate by stars and galaxies. The

**Table 4.** Number of quasar candidates, in millions, from inference on the ZTF  $g$ -band data with XGB models trained using ZTF and WISE features, at different cuts on data and minimum QSO classification probability.

data cut	QSO F1	accuracy	number of QSOs at $p_{\text{QSO}}$ higher than					
			0.3	0.5	0.8	0.9	0.95	0.99
(1)	(2)	(3)	(4)	(5)	(6)	(7)	(8)	(9)
none	0.94	0.94	45.93	32.23	11.26	6.64	4.50	2.02
$g < n_{\text{obs}}/80 + 20.375$	0.97	0.96	18.01	14.84	7.14	<b>4.85</b>	3.50	1.79
$\text{SNR} > 5\sigma \vee n_{\text{obs}} > 100$	0.97	0.96	14.59	12.24	6.18	4.28	3.13	1.66
$n_{\text{obs}} > 100$	0.97	0.96	10.96	9.46	5.00	3.53	2.63	1.44
$\text{SNR} > 5\sigma$	0.98	0.97	7.46	6.42	3.43	2.47	1.89	1.12
$\text{SNR} > 5\sigma \wedge n_{\text{obs}} > 100$	0.98	0.98	3.83	3.64	2.26	1.71	1.38	0.90

NOTE—‘Accuracy’ stands for the general three class accuracy, and both ‘QSO F1’ and ‘accuracy’ describe the test data results for a given setup of data cuts. SNR cut is applied to the  $g$ -band only. Boldface shows the suggested setup.

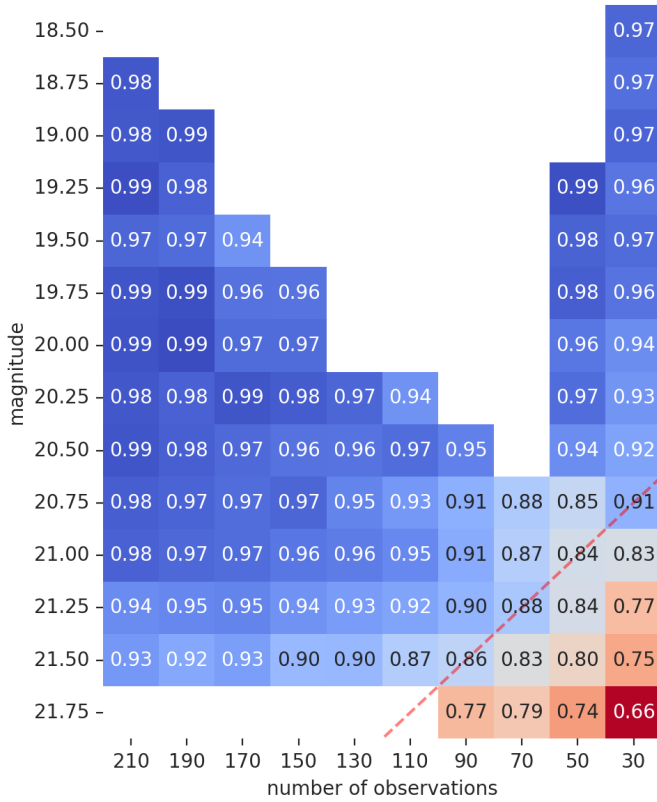


**Figure 6.** Same as fig. 3 but for XGB classification using Astromer classification, ZTF  $g$ -band median magnitudes, and WISE features. This model is used for inference in the final catalog.

photometric redshifts are available for 33% of the QZO objects with matching W[1-4] bands from AllWISE.

WISE coverage equals 41% and 77% for the inference and training data, respectively. The difference might constitute a problem, if the missing features are due to a missing sky coverage in inference data, while ML model learns on the ZTF and SDSS cross-matched footprint that missing WISE features are due to their physics and not being visible in the WISE infrared observations. We consider predictions from two XGB models, one taught on light curve classification and ZTF median magnitude, and a second one with WISE features added. The second model is the one which we use to create the QZO catalog. Among the objects with no WISE observations, and using the same cuts as in the case of QZO catalog, there are 2.8M objects classified as quasars by both of these models. However, there are also 0.65M objects classified as QSOs only by the model which does not use WISE features, and 0.31M objects classified as such only by the model which includes the WISE features, despite the fact that WISE data are only missing entries in this comparison. It is not obvious which one of these smaller samples should be accepted. The model without WISE features performs worse generally, but the model with WISE features can fail due to a misinterpretation of a meaning of missing WISE features. In the published files, described in Appendix A, we published the 0.31M sample as part of the QZO catalog, and the 0.65M sample in the file containing all objects classified as QSOs by any of the two ML models.

The difference between training and inference data in WISE coverage, as well as in distribution of magnitude

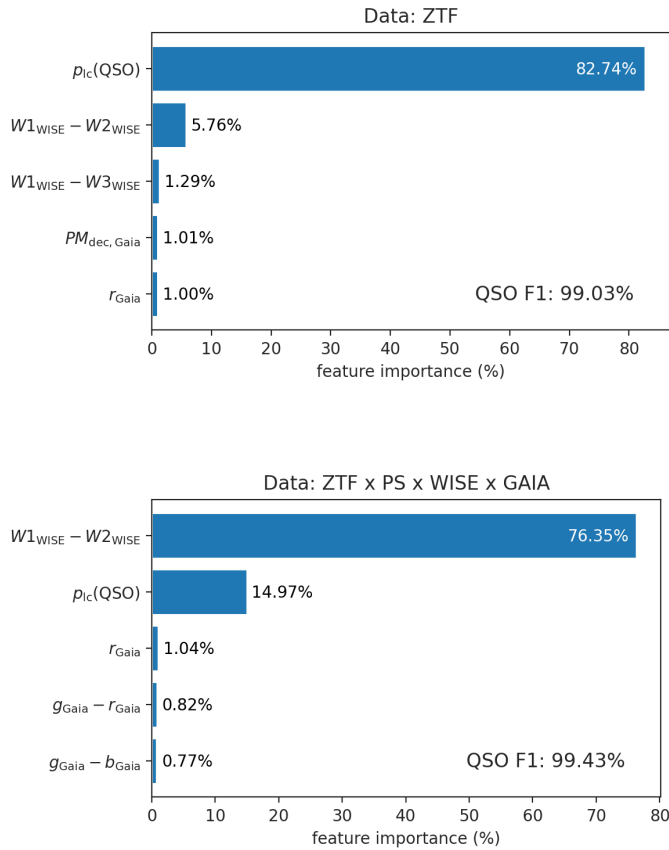


**Figure 7.** Feature importance from XGB models trained on binary QSO vs non-QSO classification problem, using the ZTF  $g$ -band data with included features from the other surveys. *Top*: ZTF training sample and processing of missing features, *bottom*: subsample of objects detected by every survey, with all the features present.  $p_{lc}(\text{QSO})$  stands for the ZTF light curves based QSO classification probability.

and number of observations (Fig. 1), can be taken into account to calibrate the QSO F1 score of the final catalog. The score can be calculated on the training data as a function of variables of interest, and then calibrated using an inference distribution of these variables. It can be achieved by cross-matching our full catalog back with SDSS, analyzing the quality of predictions on the training subset, and then calibrating the scores for any given subset of the catalog. We focus on describing the differences between the training and inference data, and how these affect the inference quality, while leaving the calibration efforts to any particular use case of our catalog.

## 5. PALOMAR SPECTROSCOPY

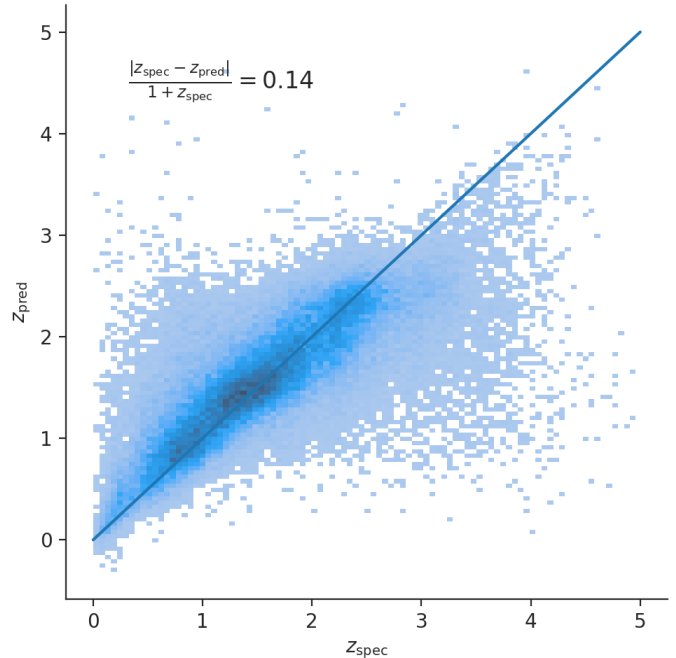


**Figure 8.** Predicted redshift estimates,  $z_{\text{pred}}$ , for the XGB model trained on ZTF  $\times$  WISE data, vs spectroscopic redshift,  $z_{\text{spec}}$ , limited to QSOs with at least 20 observation epochs. The model uses WISE magnitudes and colors, as well as ZTF  $g$ -band magnitude.

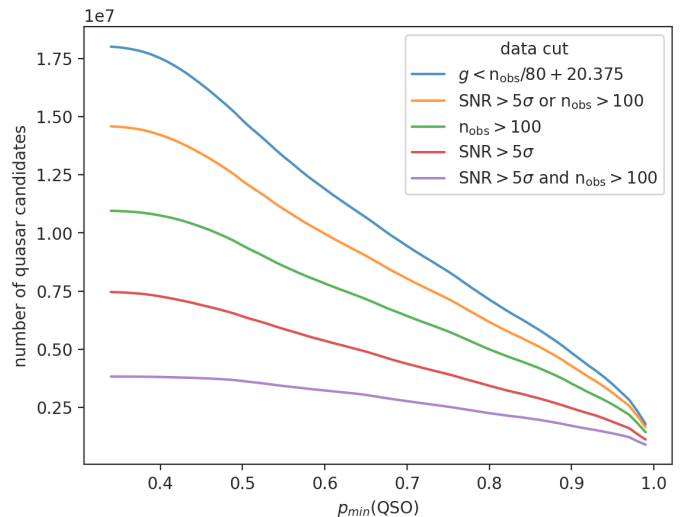


**Figure 9.** Number of QSO candidates from inference on the ZTF  $g$ -band data with XGB trained on ZTF and WISE features, as a function of minimum QSO classification probability, and grouped for different data cuts.

**Table 5.** List of random three SDSS galaxies and stars at ZTF  $g$ -band magnitude limit and number of observation epochs higher than 100, classified as AGN by our deep learning model.

SDSS				ZTF			notes
name	$z$	class	AGN	galaxy	star	light curve	
(1)	(2)	(3)	(4)	(5)	(6)	(7)	(8)
J224649.18+132545.9	0.23	galaxy	45.8%	39.1%	15.1%	fig. 11 <i>b</i>	AGN; early-type galaxy with weak [N II]
J230105.96+275256.4	0.28	galaxy	48.3%	35.5%	16.2%	fig. 11 <i>e</i>	AGN; early-type galaxy with weak [N II]
J004038.40+160949.9	0.29	galaxy	99.7%	0.3%	0.1%	fig. 11 <i>g</i>	AGN; broad H $\alpha$ emission
J002411.35-003310.9	-	star	60.5%	3.5%	36.1%	fig. 12 <i>b</i>	K5 star; MgIb and NaD absorption
J155654.47+210719.0	-	star	71.5%	9.7%	18.9%	fig. 12 <i>e</i>	CV; with strong Balmer emission
J185111.24+174645.7	-	star	74.1%	2.5%	23.4%	fig. 12 <i>g</i>	F9 star; MgIb and NaD absorption

NOTE—First two objects were observed at Palomar on 2024 Sep 11 by Daniel Stern, with 2x1200s exposure time, and clear 1.3 arcsec seeing.

We randomly selected six sources with conflicting SDSS and ZTF light curve classifications as a pilot program at Palomar Observatory on a night assigned for other science. The sample included three sources identified by SDSS as galaxies based on their spectra and three sources identified by SDSS as Galactic. All six were classified as AGN by our model. Table 5 presents these six sources, and they can be also identified in figures 11 and 12. All three SDSS Galactic sources were clearly Galactic based on the SDSS spectra, while one of the SDSS inactive galaxies was clearly active based on the SDSS spectrum.

We obtained optical spectroscopic follow-up of the other two extragalactic sources identified as inactive by SDSS, but active from the machine learning analysis of their ZTF light curves. The observations were obtained using the Double Spectrograph (DBSP, Oke & Gunn 1982) on the 5m Hale telescope at Palomar Observatory on UT 2024 September 11, which was a photometric night with  $\sim 1''.3$  seeing. For both sources, we obtained two exposures of 1200 s using the  $1''.5$  slit, the 600 line blue grating (blazed at 4000 Å), the 5500 Å dichroic, and the 316 line red grating (blazed at 7500 Å). The slits were aligned at the parallactic angle and the data were reduced using standard techniques within IRAF.

The Palomar spectra of both sources are dominated by stellar populations, showing early-type galaxies with strong absorptions from calcium H and K, the G-band, MgIb, and NaD, as well as prominent 4000 Å breaks. Both galaxies also show weak [N II] 6584 emission, indicative of a buried AGN. The SDSS spectra also show weak evidence for this nitrogen emission, which is confirmed by the Palomar data. No other strong emission lines are evident. As shown in Table 5, our model pro-

vides a probabilistic likelihood for a source being active, rather than the binary SDSS classifications. The two sources were predicted to be active at the 46-48% likelihood, and inactive at the 36-39% likelihood. Their ZTF light curves show variability by a few tenths of a magnitude since 2019 (fig. 11, panels *b* and *e*), which is somewhat surprising since the spectroscopy implies they are heavily buried, or type-2, AGN. Their optical light is expected to be dominated by their stellar populations. Indeed, the two galaxies have WISE W1-W2 colors of 0.25-0.28, indicating that their mid-IR emission are also dominated by their stellar populations (e.g., Stern et al. 2012).

The third SDSS galaxy candidate, J004038.40+160949.9, was classified with a 99.7% likelihood of being active and has varied by  $\sim 0.8$  mag since 2019. The SDSS spectrum, though classified as a starburst galaxy, shows clear broad H $\alpha$  emission and thus was not re-observed with Palomar. The first SDSS Galactic candidate, J155654.47+210719.0, shows minimal variability other than a strong flare in early 2020. The SDSS spectrum shows strong hydrogen Balmer emission and is correctly classified as a cataclysmic variable. The ML classifier identified this source with an 18.9% likelihood of being Galactic and a 71.5% likelihood of being a quasar. The other two stars show minimal variability,  $\lesssim 0.2$  mag, and are clearly normal Galactic stars based on their SDSS spectroscopy.

In summary, from this small sample, all three sources identified as Galactic by SDSS but as quasars by the ML algorithm were indeed Galactic, while all three sources identified as inactive galaxies by SDSS but as quasars by the machine learning algorithm were indeed active.

## 6. CONCLUSION

We publish a catalog of reliable QSO candidates based on time domain observations, created using deep learning classification of ZTF light curves with a transformer model, and then ensembled by XGB with WISE survey data. The high quality sample consists of 4,849,574 QSOs, with an estimated QSO F1 score of 97%. For 33% of QZO objects, with available WISE data, we publish redshifts with estimated error  $\Delta z/(1+z) = 0.14$ . We show the superiority of light curve based classification over static *griz* magnitudes and colors, and we reach similar classification capabilities to the WISE and Gaia surveys. However, both WISE and Gaia gain a significant improvement when optical light curves are added into their classifications. We also show that the ZTF light curve classifications are the most important features for QSO detection. In the case of red point-like objects detectable by both the Gaia and WISE surveys,  $W1 - W2$  is the most important feature, but the addition of light curve classification also improves the classification. We find that given at least 50 observation epochs, the QSO F1 scores deteriorate by 10pp between the objects at  $5\sigma$  SNR magnitude limit  $g \sim 20.8$  and the faintest data points at  $g \sim 21.5$ . We robustly classify objects fainter than the magnitude limit by requiring  $g < n_{\text{obs}}/80 + 20.375$ . At the ZTF 3 day median cadence, a  $\geq 900$  days time span is required to obtain a QSO F1 score higher than 90%. However, at the highest available time span of 1800 days, even a 12 day median cadence can provide similar results. Additionally, even a 500 day time span or 30 day median cadence can provide results higher than 80%.

We perform the analysis with the pre-trained Astromer transformer model. We show that the deep learning methods are necessary to fully optimize the classification with time-domain data. We successfully re-train the transformer model from ZTF DR10, on which it was originally trained, to DR20, and also successfully perform transfer learning from the ZTF *g*- to *r*-band. The usage of a pre-trained model significantly lowers the computational time, and our approach of re-training the encoder twice, first in the semi-supervised way on longer light curves, and then in the supervised manner to the SDSS classification, further improves the cores and the final training time, especially considering a vast number of re-training experiments performed. The Astromer is limited to a maximum of 200 observation epochs per light curve, and we show that the scores might improve further with longer inputs. Therefore, we conclude that our work might still not fully exploit the ZTF capabilities.

The analysis of a small sample of incorrectly classified light curves shows that the ZTF classification can even correct misclassified SDSS objects. Considering this, and the high scores obtained by our models, the next steps of the analysis involve a more nuanced approach to the QSO light curves. The possibilities include a supervised and unsupervised classification of QSOs and their subtypes, as well as a fully unsupervised search for anomalies with deep learning, using the 4.8M of objects from the QZO catalog.

A very important aspect of our analysis is that it was performed on real time domain data, which are irregularly sampled and span a wide range of available observation epochs. Our results show how much information can be extracted from the time domain surveys with deep learning. We make important conclusions from processing of the time domain data with deep learning, which can be used to help design future large time domain surveys. The catalog is ready for numerous QSO applications, and provides an important step towards a systematic search of electromagnetic counterparts to the gravitational wave events embedded in QSO accretion disks.



SJN and MJG are supported by the US National Science Foundation (NSF) through grant AST-2108402.

Based on observations obtained with the Samuel Oschin Telescope 48-inch and the 60-inch Telescope at the Palomar Observatory as part of the Zwicky Transient Facility project. ZTF is supported by the National Science Foundation under Grants No. AST-1440341 and AST-2034437 and a collaboration including current partners Caltech, IPAC, the Oskar Klein Center at Stockholm University, the University of Maryland, University of California, Berkeley, the University of Wisconsin at Milwaukee, University of Warwick, Ruhr University Bochum, Cornell University, Northwestern University and Drexel University. Operations are conducted by COO, IPAC, and UW.

Wide-field Infrared Survey Explorer, which is a joint project of the University of California, Los Angeles, and the Jet Propulsion Laboratory/California Institute of Technology, and NEOWISE, which is a project of the Jet Propulsion Laboratory/California Institute of Technology. WISE and NEOWISE are funded by the National Aeronautics and Space Administration.

European Space Agency (ESA) mission *Gaia* (<https://www.cosmos.esa.int/gaia>), processed by the Gaia Data Processing and Analysis Consortium (DPAC, <https://www.cosmos.esa.int/web/gaia/dpac/consortium>). Funding for the DPAC has been provided by national institutions, in particular the institutions participating in the Gaia Multilateral Agreement.

The Pan-STARRS1 Surveys (PS1) and the PS1 public science archive have been made possible through contributions by the Institute for Astronomy, the University of Hawaii, the Pan-STARRS Project Office, the Max-Planck Society and its participating institutes, the Max Planck Institute for Astronomy, Heidelberg and the Max Planck Institute for Extraterrestrial Physics, Garching, The Johns Hopkins University, Durham University, the University of Edinburgh, the Queen's University Belfast, the Harvard-Smithsonian Center for Astrophysics, the Las Cumbres Observatory Global Telescope Network Incorporated, the National Central University of Taiwan, the Space Telescope Science Institute, the National Aeronautics and Space Administration under Grant No. NNX08AR22G issued through the Planetary Science Division of the NASA Science Mission Directorate, the National Science Foundation Grant No. AST-1238877, the University of Maryland, Eotvos Lorand University (ELTE), the Los Alamos National Laboratory, and the Gordon and Betty Moore Foundation.

Based on observations obtained at the Hale Telescope, Palomar Observatory, as part of a collaborative agreement between the Caltech Optical Observatories and the Jet Propulsion Laboratory.

The Gordon and Betty Moore Foundation, through both the Data-Driven Investigator Program and a dedicated grant, provided critical funding for SkyPortal.

All the PS data used in this paper can be found in MAST: [10.17909/55e75e62](https://mast.stsci.org). All the ALLWISE ([Wright](https://www.ipac.caltech.edu/astro/allwise/)

*Facilities:* Zwicky Transient Facility (ZTF, [Bellm et al. 2019a](#); [Graham et al. 2019](#); [Masci et al. 2019](#); [Dekany et al. 2020](#)), Sloan Digital Sky Survey (SDSS, [Almeida et al. 2023](#)), Pan-STARRS (PS, [Chambers et al. 2016](#)), Wide-Field Infrared Survey Explorer (WISE, [Wright et al. 2010](#); [Mainzer et al. 2011](#); [Cutri et al. 2021](#)), Gaia ([Gaia Collaboration et al. 2016, 2021](#))

*Software:* Python 3 ([Van Rossum & Drake 2009](#)), Tensorflow ([Abadi et al. 2015](#)), Keras ([Chollet et al. 2015](#)), Astromer ([Donoso-Oliva et al. 2023](#)), XGBoost ([Chen & Guestrin 2016](#)), Scikit-learn ([Pedregosa et al. 2011](#)), Astropy ([Astropy Collaboration et al. 2013, 2018, 2022](#)), SkyPortal ([van der Walt et al. 2019](#); [Coughlin et al. 2023](#)), NumPy ([Harris et al. 2020](#)), SciPy ([Virtanen et al. 2020](#)), IPython ([Pérez & Granger 2007](#)), Pandas ([Wes McKinney 2010](#)), Matplotlib ([Hunter 2007](#)), seaborn ([Waskom 2021](#)), tqdm ([da Costa-Luis 2019](#))

**Table 6.** Columns present in the catalog files.

name	description
(1)	(2)
ID	ZTF identifier
ra	right ascension
dec	declination
n_obs	number of ZTF observation epochs
is_duplicate	flag indicating duplicated light curves
mag_median	ZTF <i>g</i> -band median magnitude
p_[galaxy, QSO, star]	classification probabilities
p_WISE_[galaxy, QSO, star]	classifications with added WISE data
redshift	redshift estimate

NOTE—Redshift estimate is based on WISE W[1-4] bands, and its presence indicates whether WISE data was available for a given object. The train data predictions have no ZTF identifiers and duplicate flags.

## APPENDIX

### A. PUBLISHED FILES

We publish the QZO catalog in the *QZO.csv* file, which includes 4,849,574 objects and columns as described in table 6, excluding the duplicate objects flag. The classifications are based on XGB models trained on ZTF *g*-band median magnitude and light curves classification with transformer model, as well as WISE W[1-4] magnitudes and colors. The photo-zs are based on ZTF *g*-band magnitude and WISE magnitudes and colors. We remove duplicated ZTF light curves by removing objects which within the full ZTF catalog have at least one neighbor within 1'' with more ZTF observation epochs. The final number of quasars was achieved with magnitude, number of observation epochs, and minimum quasar classification probability cuts, such that  $g < n_{\text{obs}}/80 + 20.375$ , and  $p_{\text{QSO}} > 0.9$ , where  $p_{\text{QSO}}$  is XGB classification probability for the quasar class. The photo-zs are available for 35% of these objects, depending on the availability of WISE observations.

In the file *ZTF\_all\_QSO.csv*, we publish the same columns from table 6, for 78,078,450 objects classified as QSOs by at least one of the two XGB models with and without WISE features. There are no cuts applied, and there are no duplicates removed. **26%** of objects are marked with the duplicates flag.

We publish the train data predictions in the file *train.csv*. The file contains 2,588,221 records, with ZTF ID and duplicates flag missing. Picking the longest light curve for each SDSS object removes ZTF duplicates.

### B. MISCLASSIFIED LIGHT CURVES

Figures 10, 11 and 12 show ZTF *g*-band light curves of QSOs, galaxies and stars, respectively, classified as QSOs by the XGB model based on the transformer classifications and *g*-band median magnitude. This qualitative analysis is based on a small sample of light curves, but shows interesting results. Stars classified as quasars are variable but not periodic, while galaxies classified as quasars can be actually SDSS misclassified AGNs. The QSOs misclassified as galaxies and stars generally show low amplitude variability.

## REFERENCES

- Abadi, M., Agarwal, A., Barham, P., et al. 2015, TensorFlow: Large-Scale Machine Learning on Heterogeneous Systems. <https://www.tensorflow.org/>
- Acernese, F., Agathos, M., Agatsuma, K., et al. 2015, Classical and Quantum Gravity, 32, 024001, doi: 10.1088/0264-9381/32/2/024001

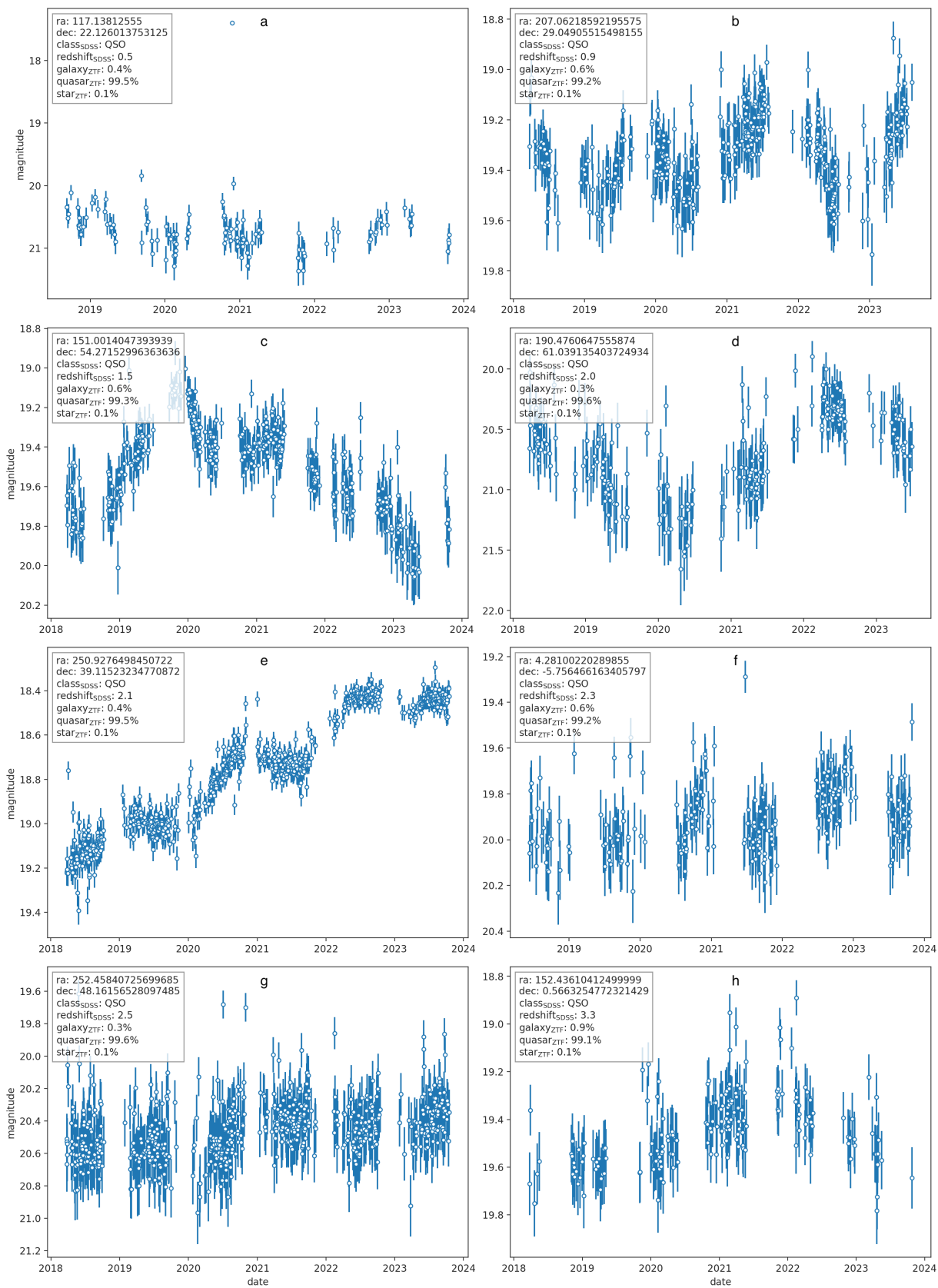
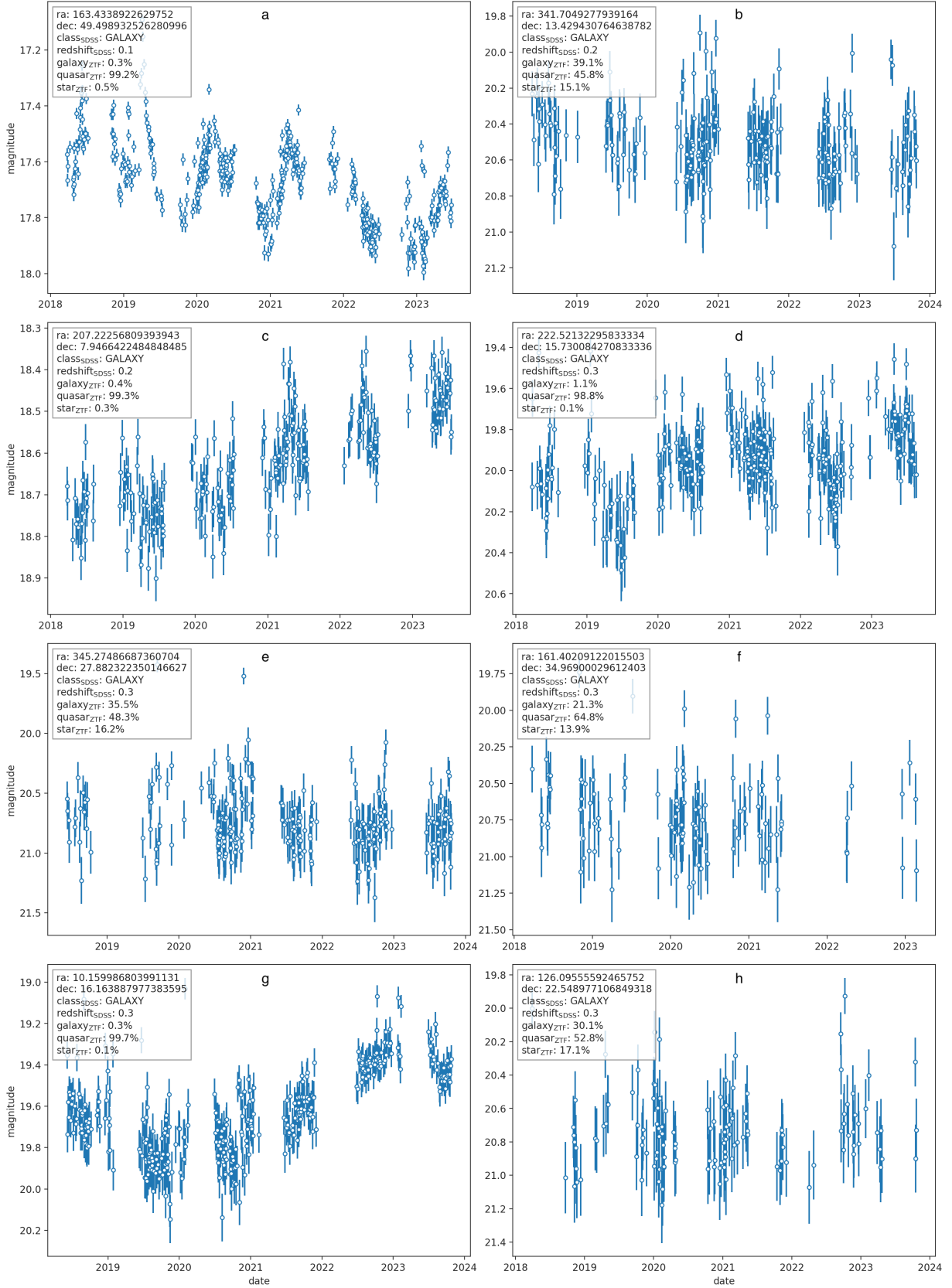


Figure 10. Random QSO ZTF  $g$ -band light curves correctly classified as QSOs by the transformer, sorted by redshift.



**Figure 11.** Random galaxy ZTF  $g$ -band light curves classified as QSOs by the transformer, sorted by redshift.

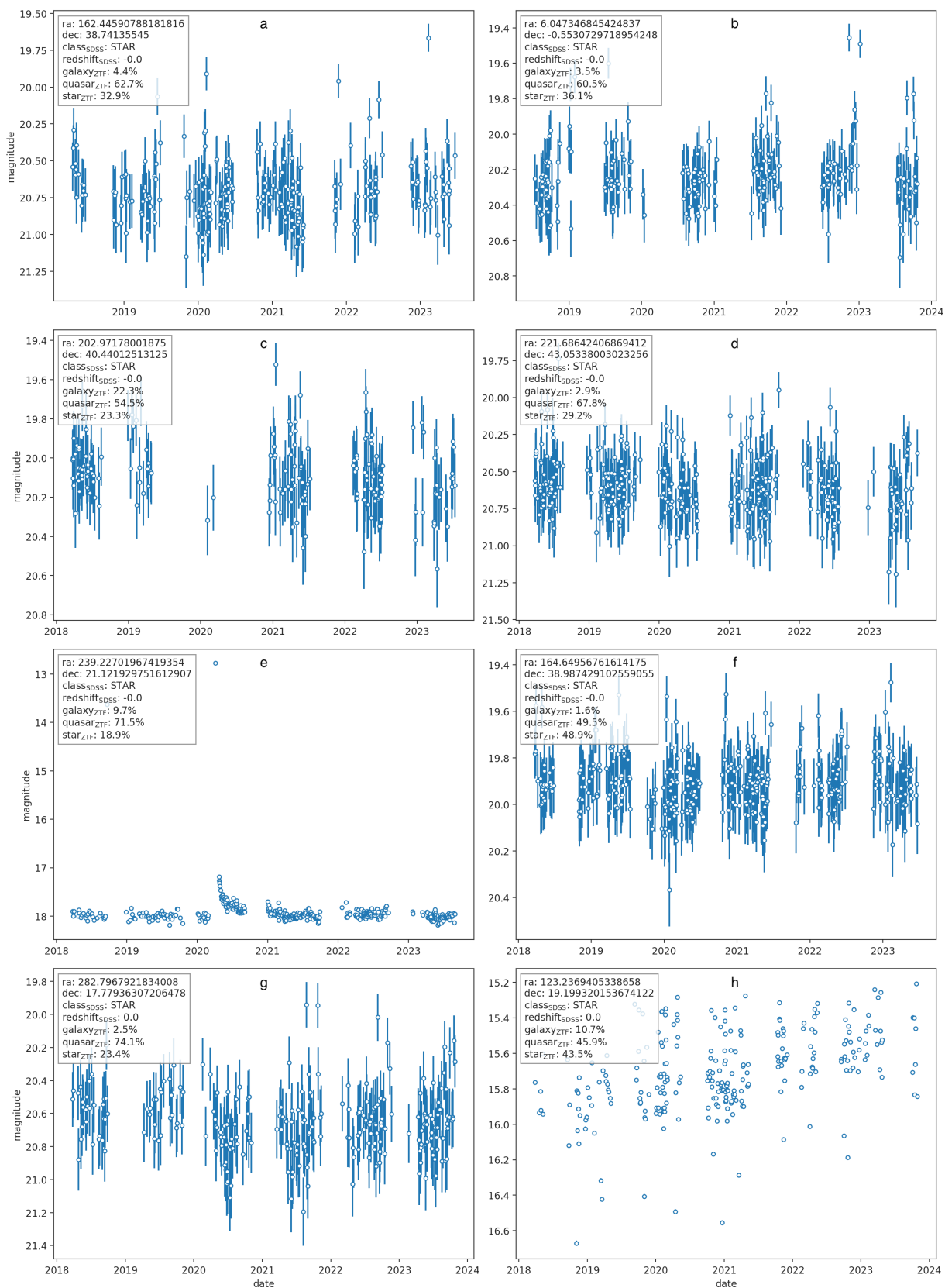


Figure 12. Random star ZTF  $g$ -band light curves incorrectly classified as QSOs by the transformer, sorted by redshift.



- Agarap, A. F. 2018, arXiv e-prints, arXiv:1803.08375, doi: [10.48550/arXiv.1803.08375](https://doi.org/10.48550/arXiv.1803.08375)
- Almeida, A., Anderson, S. F., Argudo-Fernández, M., et al. 2023, *ApJS*, 267, 44, doi: [10.3847/1538-4365/acda98](https://doi.org/10.3847/1538-4365/acda98)
- Alonso, D., Fabbian, G., Storey-Fisher, K., et al. 2023, *JCAP*, 2023, 043, doi: [10.1088/1475-7516/2023/11/043](https://doi.org/10.1088/1475-7516/2023/11/043)
- Ashton, G., Ackley, K., Hernandez, I. M., & Piotrkowski, B. 2021, *Classical and Quantum Gravity*, 38, 235004, doi: [10.1088/1361-6382/ac33bb](https://doi.org/10.1088/1361-6382/ac33bb)
- Assef, R. J., Stern, D., Noirot, G., et al. 2018, *ApJS*, 234, 23, doi: [10.3847/1538-4365/aaa00a](https://doi.org/10.3847/1538-4365/aaa00a)
- Astropy Collaboration, Robitaille, T. P., Tollerud, E. J., et al. 2013, *A&A*, 558, A33, doi: [10.1051/0004-6361/201322068](https://doi.org/10.1051/0004-6361/201322068)
- Astropy Collaboration, Price-Whelan, A. M., Sipőcz, B. M., et al. 2018, *AJ*, 156, 123, doi: [10.3847/1538-3881/aabc4f](https://doi.org/10.3847/1538-3881/aabc4f)
- Astropy Collaboration, Price-Whelan, A. M., Lim, P. L., et al. 2022, *ApJ*, 935, 167, doi: [10.3847/1538-4357/ac7c74](https://doi.org/10.3847/1538-4357/ac7c74)
- Ata, M., Baumgarten, F., Bautista, J., et al. 2017, *Monthly Notices of the Royal Astronomical Society*, 473, 4773, doi: [10.1093/mnras/stx2630](https://doi.org/10.1093/mnras/stx2630)
- Bellm, E. C., Kulkarni, S. R., Graham, M. J., et al. 2019a, *PASP*, 131, 018002, doi: [10.1088/1538-3873/aaecbe](https://doi.org/10.1088/1538-3873/aaecbe)
- Bellm, E. C., Kulkarni, S. R., Barlow, T., et al. 2019b, *PASP*, 131, 068003, doi: [10.1088/1538-3873/ab0c2a](https://doi.org/10.1088/1538-3873/ab0c2a)
- Bovy, J., Hennawi, J. F., Hogg, D. W., et al. 2011, *ApJ*, 729, 141, doi: [10.1088/0004-637X/729/2/141](https://doi.org/10.1088/0004-637X/729/2/141)
- Bovy, J., Myers, A. D., Hennawi, J. F., et al. 2012, *ApJ*, 749, 41, doi: [10.1088/0004-637X/749/1/41](https://doi.org/10.1088/0004-637X/749/1/41)
- Brescia, M., Cavuoti, S., D'Abrusco, R., Longo, G., & Mercurio, A. 2013, *ApJ*, 772, 140, doi: [10.1088/0004-637X/772/2/140](https://doi.org/10.1088/0004-637X/772/2/140)
- Brescia, M., Cavuoti, S., & Longo, G. 2015, *MNRAS*, 450, 3893, doi: [10.1093/mnras/stv854](https://doi.org/10.1093/mnras/stv854)
- Calderón Bustillo, J., Leong, S. H. W., Chandra, K., McKernan, B., & Ford, K. E. S. 2021, arXiv e-prints, arXiv:2112.12481, doi: [10.48550/arXiv.2112.12481](https://doi.org/10.48550/arXiv.2112.12481)
- Calistro Rivera, G., Lusso, E., Hennawi, J. F., & Hogg, D. W. 2016, *ApJ*, 833, 98, doi: [10.3847/1538-4357/833/1/98](https://doi.org/10.3847/1538-4357/833/1/98)
- Carrasco, D., Barrientos, L. F., Pichara, K., et al. 2015, *A&A*, 584, A44, doi: [10.1051/0004-6361/201525752](https://doi.org/10.1051/0004-6361/201525752)
- Castorina, E., Hand, N., Seljak, U., et al. 2019, *Journal of Cosmology and Astroparticle Physics*, 2019, 010, doi: [10.1088/1475-7516/2019/09/010](https://doi.org/10.1088/1475-7516/2019/09/010)
- Chambers, K. C., Magnier, E. A., Metcalfe, N., et al. 2016, arXiv e-prints, arXiv:1612.05560, doi: [10.48550/arXiv.1612.05560](https://doi.org/10.48550/arXiv.1612.05560)
- Chen, H.-Y., Haster, C.-J., Vitale, S., Farr, W. M., & Isi, M. 2022, *MNRAS*, 513, 2152, doi: [10.1093/mnras/stac989](https://doi.org/10.1093/mnras/stac989)
- Chen, T., & Guestrin, C. 2016, in *Proceedings of the 22Nd ACM SIGKDD International Conference on Knowledge Discovery and Data Mining, KDD '16 (New York, NY, USA: ACM)*, 785–794, doi: [10.1145/2939672.2939785](https://doi.org/10.1145/2939672.2939785)
- Chollet, F., et al. 2015, *Keras*, <https://keras.io>
- Ciesla, L., Charmandaris, V., Georgakakis, A., et al. 2015, *A&A*, 576, A10, doi: [10.1051/0004-6361/201425252](https://doi.org/10.1051/0004-6361/201425252)
- Collaboration, G. 2020, *Gaia Source Catalogue eDR3*, *IPAC*, doi: [10.26131/IRSA541](https://doi.org/10.26131/IRSA541)
- Coughlin, M. W., Burdge, K., Duev, D. A., et al. 2021, *MNRAS*, 505, 2954, doi: [10.1093/mnras/stab1502](https://doi.org/10.1093/mnras/stab1502)
- Coughlin, M. W., Bloom, J. S., Nir, G., et al. 2023, *The Astrophysical Journal Supplement Series*, 267, 31, doi: [10.3847/1538-4365/acdee1](https://doi.org/10.3847/1538-4365/acdee1)
- Croom, S. M., Smith, R. J., Boyle, B. J., et al. 2004, *MNRAS*, 349, 1397, doi: [10.1111/j.1365-2966.2004.07619.x](https://doi.org/10.1111/j.1365-2966.2004.07619.x)
- Croom, S. M., Richards, G. T., Shanks, T., et al. 2009, *MNRAS*, 392, 19, doi: [10.1111/j.1365-2966.2008.14052.x](https://doi.org/10.1111/j.1365-2966.2008.14052.x)
- Cuoco, A., Bilicki, M., Xia, J.-Q., & Branchini, E. 2017, *ApJS*, 232, 10, doi: [10.3847/1538-4365/aa8553](https://doi.org/10.3847/1538-4365/aa8553)
- Curran, S. J. 2020, *MNRAS*, 493, L70, doi: [10.1093/mnrasl/slaa012](https://doi.org/10.1093/mnrasl/slaa012)
- Cutri, R. M., Wright, E. L., Conrow, T., et al. 2021, *VizieR Online Data Catalog: AllWISE Data Release (Cutri+ 2013)*, *VizieR On-line Data Catalog: II/328*. Originally published in: *IPAC/Caltech (2013)*
- da Costa-Luis, C. 2019, *The Journal of Open Source Software*, 4, 1277, doi: [10.21105/joss.01277](https://doi.org/10.21105/joss.01277)
- Dam, L., Lewis, G. F., & Brewer, B. J. 2023, *MNRAS*, 525, 231, doi: [10.1093/mnras/stad2322](https://doi.org/10.1093/mnras/stad2322)
- de Jong, R. S., Agertz, O., Berbel, A. A., et al. 2019, *The Messenger*, 175, 3, doi: [10.18727/0722-6691/5117](https://doi.org/10.18727/0722-6691/5117)
- Dekany, R., Smith, R. M., Riddle, R., et al. 2020, *PASP*, 132, 038001, doi: [10.1088/1538-3873/ab4ca2](https://doi.org/10.1088/1538-3873/ab4ca2)
- DESI Collaboration, Aghamousa, A., Aguilar, J., et al. 2016, arXiv e-prints. <https://arxiv.org/abs/1611.00036>
- DiPompeo, M. A., Bovy, J., Myers, A. D., & Lang, D. 2015, *MNRAS*, 452, 3124, doi: [10.1093/mnras/stv1562](https://doi.org/10.1093/mnras/stv1562)
- DiPompeo, M. A., Hickox, R. C., Eftekharzadeh, S., & Myers, A. D. 2017, *MNRAS*, 469, 4630, doi: [10.1093/mnras/stx1215](https://doi.org/10.1093/mnras/stx1215)
- DiPompeo, M. A., Hickox, R. C., & Myers, A. D. 2016, *MNRAS*, 456, 924, doi: [10.1093/mnras/stv2681](https://doi.org/10.1093/mnras/stv2681)
- DiPompeo, M. A., Myers, A. D., Hickox, R. C., Geach, J. E., & Hainline, K. N. 2014, *MNRAS*, 442, 3443, doi: [10.1093/mnras/stu1115](https://doi.org/10.1093/mnras/stu1115)
- Donoso-Oliva, C., Becker, I., Protopapas, P., et al. 2023, *A&A*, 670, A54, doi: [10.1051/0004-6361/202243928](https://doi.org/10.1051/0004-6361/202243928)

- Drake, A. J., Graham, M. J., Djorgovski, S. G., et al. 2014, *ApJS*, 213, 9, doi: [10.1088/0067-0049/213/1/9](https://doi.org/10.1088/0067-0049/213/1/9)
- Drake, A. J., Djorgovski, S. G., Catelan, M., et al. 2017, *MNRAS*, 469, 3688, doi: [10.1093/mnras/stx1085](https://doi.org/10.1093/mnras/stx1085)
- Edelson, R., & Malkan, M. 2012, *ApJ*, 751, 52, doi: [10.1088/0004-637X/751/1/52](https://doi.org/10.1088/0004-637X/751/1/52)
- Eftekharzadeh, S., Myers, A. D., White, M., et al. 2015, *MNRAS*, 453, 2779, doi: [10.1093/mnras/stv1763](https://doi.org/10.1093/mnras/stv1763)
- Fotopoulou, S., & Paltani, S. 2018, *A&A*, 619, A14, doi: [10.1051/0004-6361/201730763](https://doi.org/10.1051/0004-6361/201730763)
- Fotopoulou, S., Picaud, F., Paltani, S., et al. 2016, *A&A*, 592, A5, doi: [10.1051/0004-6361/201527402](https://doi.org/10.1051/0004-6361/201527402)
- Gaia Collaboration, Prusti, T., de Bruijne, J. H. J., et al. 2016, *A&A*, 595, A1, doi: [10.1051/0004-6361/201629272](https://doi.org/10.1051/0004-6361/201629272)
- Gaia Collaboration, Brown, A. G. A., Vallenari, A., et al. 2021, *A&A*, 649, A1, doi: [10.1051/0004-6361/202039657](https://doi.org/10.1051/0004-6361/202039657)
- García-García, C., Ruiz-Zapatero, J., Alonso, D., et al. 2021, *JCAP*, 2021, 030, doi: [10.1088/1475-7516/2021/10/030](https://doi.org/10.1088/1475-7516/2021/10/030)
- García-Jara, G., Protopapas, P., & Estévez, P. A. 2022, *ApJ*, 935, 23, doi: [10.3847/1538-4357/ac6f5a](https://doi.org/10.3847/1538-4357/ac6f5a)
- Gezari, S. 2021, *ARA&A*, 59, 21, doi: [10.1146/annurev-astro-111720-030029](https://doi.org/10.1146/annurev-astro-111720-030029)
- Godines, D., Bachelet, E., Narayan, G., & Street, R. A. 2019, *Astronomy and Computing*, 28, 100298, doi: [10.1016/j.ascom.2019.100298](https://doi.org/10.1016/j.ascom.2019.100298)
- Gomez, S., Villar, V. A., Berger, E., et al. 2023, *ApJ*, 949, 113, doi: [10.3847/1538-4357/acc535](https://doi.org/10.3847/1538-4357/acc535)
- Graham, M. J., Kulkarni, S. R., Bellm, E. C., et al. 2019, *PASP*, 131, 078001, doi: [10.1088/1538-3873/ab006c](https://doi.org/10.1088/1538-3873/ab006c)
- Graham, M. J., Ford, K. E. S., McKernan, B., et al. 2020, *PhRvL*, 124, 251102, doi: [10.1103/PhysRevLett.124.251102](https://doi.org/10.1103/PhysRevLett.124.251102)
- Graham, M. J., McKernan, B., Ford, K. E. S., et al. 2023, *ApJ*, 942, 99, doi: [10.3847/1538-4357/aca480](https://doi.org/10.3847/1538-4357/aca480)
- Harris, C. R., Millman, K. J., van der Walt, S. J., et al. 2020, *Nature*, 585, 357, doi: [10.1038/s41586-020-2649-2](https://doi.org/10.1038/s41586-020-2649-2)
- Healy, B. F., Coughlin, M. W., Mahabal, A. A., et al. 2024, *ApJS*, 272, 14, doi: [10.3847/1538-4365/ad33c6](https://doi.org/10.3847/1538-4365/ad33c6)
- Ho, S., Agarwal, N., Myers, A. D., et al. 2015, *JCAP*, 5, 040, doi: [10.1088/1475-7516/2015/05/040](https://doi.org/10.1088/1475-7516/2015/05/040)
- Hochreiter, S., & Schmidhuber, J. 1997, *Neural computation*, 9, 1735
- Hoffman, D. L., Harrison, T. E., & McNamara, B. J. 2009, *AJ*, 138, 466, doi: [10.1088/0004-6256/138/2/466](https://doi.org/10.1088/0004-6256/138/2/466)
- Hou, J., Sánchez, A. G., Ross, A. J., et al. 2020, *Monthly Notices of the Royal Astronomical Society*, 500, 1201, doi: [10.1093/mnras/staa3234](https://doi.org/10.1093/mnras/staa3234)
- Hunter, J. D. 2007, *Computing in Science & Engineering*, 9, 90, doi: [10.1109/MCSE.2007.55](https://doi.org/10.1109/MCSE.2007.55)
- Ivezić, Ž. 2016, *Proceedings of the International Astronomical Union*, 12, 330–337, doi: [10.1017/S1743921316012424](https://doi.org/10.1017/S1743921316012424)
- Jayasinghe, T., Kochanek, C. S., Stanek, K. Z., et al. 2018, *MNRAS*, 477, 3145, doi: [10.1093/mnras/sty838](https://doi.org/10.1093/mnras/sty838)
- Kelly, B. C., Bechtold, J., & Siemiginowska, A. 2009, *ApJ*, 698, 895, doi: [10.1088/0004-637X/698/1/895](https://doi.org/10.1088/0004-637X/698/1/895)
- Kimura, S. S., Murase, K., & Bartos, I. 2021, *ApJ*, 916, 111, doi: [10.3847/1538-4357/ac0535](https://doi.org/10.3847/1538-4357/ac0535)
- Kochanek, C. S., Shappee, B. J., Stanek, K. Z., et al. 2017, *PASP*, 129, 104502, doi: [10.1088/1538-3873/aa80d9](https://doi.org/10.1088/1538-3873/aa80d9)
- Kormendy, J., & Ho, L. C. 2013, *ARA&A*, 51, 511, doi: [10.1146/annurev-astro-082708-101811](https://doi.org/10.1146/annurev-astro-082708-101811)
- Kozłowski, S., Kochanek, C. S., Udalski, A., et al. 2010, *ApJ*, 708, 927, doi: [10.1088/0004-637X/708/2/927](https://doi.org/10.1088/0004-637X/708/2/927)
- Krolewski, A., Percival, W. J., Ferraro, S., et al. 2024, *Journal of Cosmology and Astroparticle Physics*, 2024, 021, doi: [10.1088/1475-7516/2024/03/021](https://doi.org/10.1088/1475-7516/2024/03/021)
- Kunsági-Máté, S., Beck, R., Szapudi, I., & Csabai, I. 2022, *Monthly Notices of the Royal Astronomical Society*, 516, 2662, doi: [10.1093/mnras/stac2411](https://doi.org/10.1093/mnras/stac2411)
- Kurcz, A., Bilicki, M., Solarz, A., et al. 2016, *A&A*, 592, A25, doi: [10.1051/0004-6361/201628142](https://doi.org/10.1051/0004-6361/201628142)
- Lang, D. 2014, *The Astronomical Journal*, 147, 108, doi: [10.1088/0004-6256/147/5/108](https://doi.org/10.1088/0004-6256/147/5/108)
- Laurent, P., Eftekharzadeh, S., Le Goff, J.-M., et al. 2017, *JCAP*, 7, 017, doi: [10.1088/1475-7516/2017/07/017](https://doi.org/10.1088/1475-7516/2017/07/017)
- Law, N. M., Kulkarni, S. R., Dekany, R. G., et al. 2009, *PASP*, 121, 1395, doi: [10.1086/648598](https://doi.org/10.1086/648598)
- Leistedt, B., Peiris, H. V., & Roth, N. 2014, *Phys. Rev. Lett.*, 113, 221301, doi: [10.1103/PhysRevLett.113.221301](https://doi.org/10.1103/PhysRevLett.113.221301)
- LIGO Scientific Collaboration, Aasi, J., Abbott, B. P., et al. 2015, *Classical and Quantum Gravity*, 32, 074001, doi: [10.1088/0264-9381/32/7/074001](https://doi.org/10.1088/0264-9381/32/7/074001)
- Lindgren, L., Hernández, J., Bombrun, A., et al. 2018, *A&A*, 616, A2, doi: [10.1051/0004-6361/201832727](https://doi.org/10.1051/0004-6361/201832727)
- Logan, C. H. A., & Fotopoulou, S. 2020, *A&A*, 633, A154, doi: [10.1051/0004-6361/201936648](https://doi.org/10.1051/0004-6361/201936648)
- Lusso, E., Risaliti, G., Nardini, E., et al. 2020, *A&A*, 642, A150, doi: [10.1051/0004-6361/202038899](https://doi.org/10.1051/0004-6361/202038899)
- Lyke, B. W., Higley, A. N., McLane, J. N., et al. 2020, *ApJS*, 250, 8, doi: [10.3847/1538-4365/aba623](https://doi.org/10.3847/1538-4365/aba623)
- MacLeod, C. L., Ivezić, Ž., Kochanek, C. S., et al. 2010, *ApJ*, 721, 1014, doi: [10.1088/0004-637X/721/2/1014](https://doi.org/10.1088/0004-637X/721/2/1014)
- Maddox, N., Hewett, P. C., Warren, S. J., & Croom, S. M. 2008, *MNRAS*, 386, 1605, doi: [10.1111/j.1365-2966.2008.13138.x](https://doi.org/10.1111/j.1365-2966.2008.13138.x)
- Mainzer, A., Bauer, J., Grav, T., et al. 2011, *ApJ*, 731, 53, doi: [10.1088/0004-637X/731/1/53](https://doi.org/10.1088/0004-637X/731/1/53)

- Malek, K., Buat, V., Burgarella, D., et al. 2020, in IAU Symposium, Vol. 341, IAU Symposium, ed. M. Boquien, E. Lusso, C. Gruppioni, & P. Tissera, 39–43, doi: [10.1017/S174392131900471X](https://doi.org/10.1017/S174392131900471X)
- Masci, F. J., Laher, R. R., Rusholme, B., et al. 2019, PASP, 131, 018003, doi: [10.1088/1538-3873/aae8ac](https://doi.org/10.1088/1538-3873/aae8ac)
- McKernan, B., Ford, K. E. S., Bartos, I., et al. 2019, ApJL, 884, L50, doi: [10.3847/2041-8213/ab4886](https://doi.org/10.3847/2041-8213/ab4886)
- Ménard, B., & Bartelmann, M. 2002, A&A, 386, 784, doi: [10.1051/0004-6361:20020274](https://doi.org/10.1051/0004-6361:20020274)
- Merloni, A., Alexander, D. A., Banerji, M., et al. 2019, The Messenger, 175, 42, doi: [10.18727/0722-6691/5125](https://doi.org/10.18727/0722-6691/5125)
- Mistry, D., Copperwheat, C. M., Darnley, M. J., & Olier, I. 2022, Monthly Notices of the Royal Astronomical Society, 517, 3362, doi: [10.1093/mnras/stac2760](https://doi.org/10.1093/mnras/stac2760)
- Mukherjee, S., Ghosh, A., Graham, M. J., et al. 2020, arXiv e-prints, arXiv:2009.14199, doi: [10.48550/arXiv.2009.14199](https://doi.org/10.48550/arXiv.2009.14199)
- Nakoneczny, S., Bilicki, M., Solarz, A., et al. 2019, A&A, 624, A13, doi: [10.1051/0004-6361/201834794](https://doi.org/10.1051/0004-6361/201834794)
- Nakoneczny, S. J., Bilicki, M., Pollo, A., et al. 2021, A&A, 649, A81, doi: [10.1051/0004-6361/202039684](https://doi.org/10.1051/0004-6361/202039684)
- Oke, J. B., & Gunn, J. E. 1982, PASP, 94, 586, doi: [10.1086/131027](https://doi.org/10.1086/131027)
- Palmese, A., Fishbach, M., Burke, C. J., Annis, J., & Liu, X. 2021, ApJL, 914, L34, doi: [10.3847/2041-8213/ac0883](https://doi.org/10.3847/2041-8213/ac0883)
- Pasquet-Itam, J., & Pasquet, J. 2018, A&A, 611, A97, doi: [10.1051/0004-6361/201731106](https://doi.org/10.1051/0004-6361/201731106)
- Pedregosa, F., Varoquaux, G., Gramfort, A., et al. 2011, Journal of Machine Learning Research, 12, 2825
- Pérez, F., & Granger, B. E. 2007, Computing in Science and Engineering, 9, 21, doi: [10.1109/MCSE.2007.53](https://doi.org/10.1109/MCSE.2007.53)
- Perna, R., Lazzati, D., & Cantiello, M. 2021, ApJL, 906, L7, doi: [10.3847/2041-8213/abd319](https://doi.org/10.3847/2041-8213/abd319)
- Pojmanski, G. 2002, AcA, 52, 397, doi: [10.48550/arXiv.astro-ph/0210283](https://doi.org/10.48550/arXiv.astro-ph/0210283)
- Rees, M. J. 1988, Nature, 333, 523, doi: [10.1038/333523a0](https://doi.org/10.1038/333523a0)
- Rehemtulla, N., & Miller, A. 2023, in American Astronomical Society Meeting Abstracts, Vol. 241, American Astronomical Society Meeting Abstracts, 105.30
- Richard, J., Kneib, J. P., Blake, C., et al. 2019, The Messenger, 175, 50, doi: [10.18727/0722-6691/5127](https://doi.org/10.18727/0722-6691/5127)
- Richards, G. T., Nichol, R. C., Gray, A. G., et al. 2004, ApJS, 155, 257, doi: [10.1086/425356](https://doi.org/10.1086/425356)
- Richards, G. T., Myers, A. D., Gray, A. G., et al. 2009a, ApJS, 180, 67, doi: [10.1088/0067-0049/180/1/67](https://doi.org/10.1088/0067-0049/180/1/67)
- Richards, G. T., Deo, R. P., Lacy, M., et al. 2009b, AJ, 137, 3884, doi: [10.1088/0004-6256/137/4/3884](https://doi.org/10.1088/0004-6256/137/4/3884)
- Richards, G. T., Myers, A. D., Peters, C. M., et al. 2015, ApJS, 219, 39, doi: [10.1088/0067-0049/219/2/39](https://doi.org/10.1088/0067-0049/219/2/39)
- Richards, J. W., Starr, D. L., Butler, N. R., et al. 2011, ApJ, 733, 10, doi: [10.1088/0004-637X/733/1/10](https://doi.org/10.1088/0004-637X/733/1/10)
- Risaliti, G., & Lusso, E. 2015, The Astrophysical Journal, 815, 33, doi: [10.1088/0004-637X/815/1/33](https://doi.org/10.1088/0004-637X/815/1/33)
- Salvato, M., Hasinger, G., Ilbert, O., et al. 2009, ApJ, 690, 1250, doi: [10.1088/0004-637X/690/2/1250](https://doi.org/10.1088/0004-637X/690/2/1250)
- Salvato, M., Ilbert, O., Hasinger, G., et al. 2011, ApJ, 742, 61, doi: [10.1088/0004-637X/742/2/61](https://doi.org/10.1088/0004-637X/742/2/61)
- Scranton, R., Ménard, B., Richards, G. T., et al. 2005, ApJ, 633, 589, doi: [10.1086/431358](https://doi.org/10.1086/431358)
- Secrest, N. J., Dudik, R. P., Dorland, B. N., et al. 2015, ApJS, 221, 12, doi: [10.1088/0067-0049/221/1/12](https://doi.org/10.1088/0067-0049/221/1/12)
- Secrest, N. J., von Hausegger, S., Rameez, M., et al. 2021, ApJL, 908, L51, doi: [10.3847/2041-8213/abdd40](https://doi.org/10.3847/2041-8213/abdd40)
- Setti, G., & Woltjer, L. 1973, ApJL, 181, L61, doi: [10.1086/181185](https://doi.org/10.1086/181185)
- Sherwin, B. D., Das, S., Hajian, A., et al. 2012, PhRvD, 86, 083006, doi: [10.1103/PhysRevD.86.083006](https://doi.org/10.1103/PhysRevD.86.083006)
- Shu, Y., Koposov, S. E., Evans, N. W., et al. 2019, Monthly Notices of the Royal Astronomical Society, 489, 4741, doi: [10.1093/mnras/stz2487](https://doi.org/10.1093/mnras/stz2487)
- Stachie, C., Coughlin, M. W., Christensen, N., & Muthukrishna, D. 2020, MNRAS, 497, 1320, doi: [10.1093/mnras/staa1776](https://doi.org/10.1093/mnras/staa1776)
- Stalevski, M., Ricci, C., Ueda, Y., et al. 2016, MNRAS, 458, 2288, doi: [10.1093/mnras/stw444](https://doi.org/10.1093/mnras/stw444)
- Stein, R., Mahabal, A., Reusch, S., et al. 2024, ApJL, 965, L14, doi: [10.3847/2041-8213/ad3337](https://doi.org/10.3847/2041-8213/ad3337)
- Stern, D., Assef, R. J., Benford, D. J., et al. 2012, ApJ, 753, 30, doi: [10.1088/0004-637X/753/1/30](https://doi.org/10.1088/0004-637X/753/1/30)
- Stözlner, B., Cuoco, A., Lesgourgues, J., & Bilicki, M. 2018, PhRvD, 97, 063506, doi: [10.1103/PhysRevD.97.063506](https://doi.org/10.1103/PhysRevD.97.063506)
- Storey-Fisher, K., Hogg, D. W., Rix, H.-W., et al. 2024, ApJ, 964, 69, doi: [10.3847/1538-4357/ad1328](https://doi.org/10.3847/1538-4357/ad1328)
- van der Walt, S. J., Crellin-Quick, A., & Bloom, J. S. 2019, Journal of Open Source Software, 4, 1247, doi: [10.21105/joss.01247](https://doi.org/10.21105/joss.01247)
- van Roestel, J., Duev, D. A., Mahabal, A. A., et al. 2021, AJ, 161, 267, doi: [10.3847/1538-3881/abe853](https://doi.org/10.3847/1538-3881/abe853)
- Van Rossum, G., & Drake, F. L. 2009, Python 3 Reference Manual (Scotts Valley, CA: CreateSpace)
- Virtanen, P., Gommers, R., Oliphant, T. E., et al. 2020, Nature Methods, 17, 261, doi: [10.1038/s41592-019-0686-2](https://doi.org/10.1038/s41592-019-0686-2)
- Wang, J.-M., Liu, J.-R., Ho, L. C., Li, Y.-R., & Du, P. 2021, ApJL, 916, L17, doi: [10.3847/2041-8213/ac0b46](https://doi.org/10.3847/2041-8213/ac0b46)
- Warren, S. J., Hewett, P. C., & Foltz, C. B. 2000, MNRAS, 312, 827, doi: [10.1046/j.1365-8711.2000.03206.x](https://doi.org/10.1046/j.1365-8711.2000.03206.x)

- Waskom, M. L. 2021, *Journal of Open Source Software*, 6, 3021, doi: [10.21105/joss.03021](https://doi.org/10.21105/joss.03021)
- Wes McKinney. 2010, in *Proceedings of the 9th Python in Science Conference*, ed. Stéfan van der Walt & Jarrod Millman, 56 – 61, doi: [10.25080/Majora-92bf1922-00a](https://doi.org/10.25080/Majora-92bf1922-00a)
- Woźniak, P. R., Vestrand, W. T., Akerlof, C. W., et al. 2004, *AJ*, 127, 2436, doi: [10.1086/382719](https://doi.org/10.1086/382719)
- Wright, E. L., Eisenhardt, P. R. M., Mainzer, A. K., et al. 2010, *AJ*, 140, 1868, doi: [10.1088/0004-6256/140/6/1868](https://doi.org/10.1088/0004-6256/140/6/1868)
- Wright, E. L., Eisenhardt, P. R. M., Mainzer, A. K., et al. 2019, *AllWISE Source Catalog*, IPAC, doi: [10.26131/IRSA1](https://doi.org/10.26131/IRSA1)
- Wu, X.-B., Hao, G., Jia, Z., Zhang, Y., & Peng, N. 2012, *AJ*, 144, 49, doi: [10.1088/0004-6256/144/2/49](https://doi.org/10.1088/0004-6256/144/2/49)
- Yahata, K., Suto, Y., Kayo, I., et al. 2005, *Publications of the Astronomical Society of Japan*, 57, 529, doi: [10.1093/pasj/57.4.529](https://doi.org/10.1093/pasj/57.4.529)
- Yang, G., Boquien, M., Buat, V., et al. 2020, *MNRAS*, 491, 740, doi: [10.1093/mnras/stz3001](https://doi.org/10.1093/mnras/stz3001)
- Yang, Q., Wu, X.-B., Fan, X., et al. 2017, *AJ*, 154, 269, doi: [10.3847/1538-3881/aa943c](https://doi.org/10.3847/1538-3881/aa943c)
- York, D. G., Adelman, J., Anderson, Jr., J. E., et al. 2000, *AJ*, 120, 1579, doi: [10.1086/301513](https://doi.org/10.1086/301513)
- Zarrouk, P., Rezaie, M., Raichoor, A., et al. 2021, *Monthly Notices of the Royal Astronomical Society*, 503, 2562, doi: [10.1093/mnras/stab298](https://doi.org/10.1093/mnras/stab298)